

Enhancing the PEC Efficiency in the Perspective of Crystal Facet Engineering and Modulation of Surfaces

Sudipa Manna, Ashis Kumar Satpati,* Chandra Nath Patra, and Avesh Kumar Tyagi*



Cite This: *ACS Omega* 2024, 9, 6128–6146



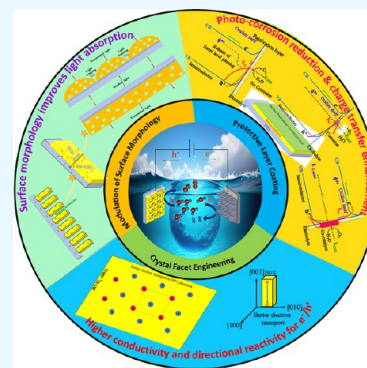
Read Online

ACCESS |

Metrics & More

Article Recommendations

ABSTRACT: Generation of hydrogen is one of the most promising routes to harvest solar energy for its sustainable utilization. Among different routes, the photoelectrochemical (PEC) process to split water using solar light to produce hydrogen is the green method to generate hydrogen. The sluggish kinetics through complicated pathways makes the oxygen evolution reaction the rate limiting step of the overall water splitting process. Therefore, development of an efficient photoanode for the sustainable oxidation of water is most challenging in an efficient overall PEC water splitting process. The low solar to hydrogen conversion efficiency arises from the slow surface kinetics, poor hole diffusion, and fast charge recombination processes. There have been strategies to improve catalytic performances through the removal of such detrimental effects. The generation of engineered surfaces is one of the important strategies recently adopted for the enhancement of the catalytic efficiencies. The present review has been focused on the discussion of engineered surfaces using crystal facet engineering, protective surface layer, passivation using the atomic layer deposition (ALD) technique, and cocatalyst modified surfaces to enhance the catalytic efficiency. Some of the important parameters defining catalyst performance are also discussed at the beginning of the review.



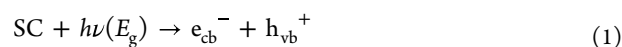
1. INTRODUCTION

The human development index or in general the well-being of the citizens of a country is strongly correlated to the per capita energy consumption. According to the International Energy Agency report, the global electricity demand in 2019 alone stands at ~ 22.8 TWh, up by 1.7% compared to 2018.¹ With the ever-increasing use of conventional fuels like oil, gas, and coal for energy generation, carbon dioxide emissions are shooting up and creating an environmental imbalance which threatens the biodiversity of the whole planet. In 2021, 36.4 Gtons of carbon dioxide gas was released into the atmosphere due to anthropogenic activities.² With the rise in greenhouse gases, the rise in the average temperature of the earth and rising sea levels pose an existential threat for the sole livable planet. It is high time to take necessary actions to limit the cause at its very root. Out of several important renewable energy sources, the unlimited availability of solar energy (1.73×10^5 TW every day on earth) has been an important source to choose as the most preferred choice. The conversion of solar energy into hydrogen is the most attractive option as hydrogen has the highest energy density (141.9 MJ kg^{-1}) and can be produced from water. Furthermore, upon combustion of H_2 the end product is water, thereby forming a zero-carbon footprint loop of energy production. However, the availability of efficient commercial methods to convert solar energy to electrical energy remains a challenge. Hydrogen can be produced from water using solar energy through two important pathways—photocatalysis (PC) and photoelectrocatalysis (PEC)—and in the scientific

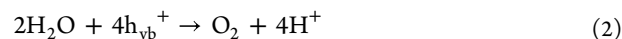
literature both processes are generally named “water splitting”. Both methods have important utilities in the generation of hydrogen from water. Water splitting is a thermodynamically energy intensive process and requires 237.2 kJ mol^{-1} of energy to convert water into hydrogen and oxygen. Theoretically, 1.23 V should be sufficient for the electrolysis of water; however, an overpotential of 1.6 – 2.4 V for both the hydrogen evolution reaction (HER) and the oxygen evolution reaction (OER) is required to drive the overall process.

The mechanism of photocatalytic water splitting over a semiconductor (SC) electrode is as follows:

absorption of light:



OER:



Received: October 9, 2023

Revised: January 5, 2024

Accepted: January 11, 2024

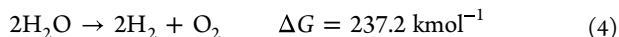
Published: January 31, 2024



HER:

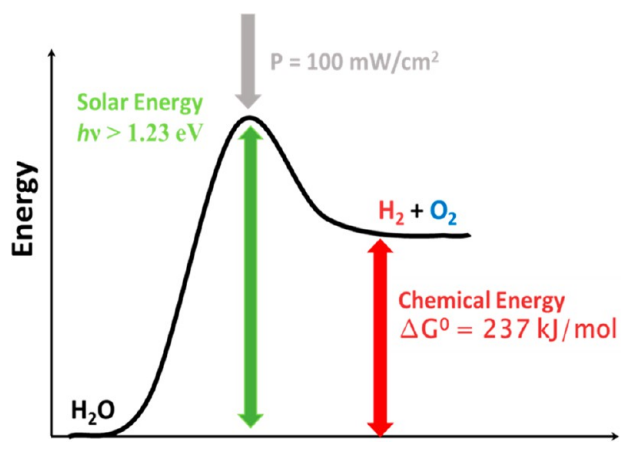


overall water splitting reaction:



The energetics of the different steps of the water splitting process are indicated in Scheme 1

Scheme 1. Energy Level Diagram Depicting Energy Requirements of the Water Splitting Process



Light is absorbed by the SC to produce an electron/hole pair, which converts water into hydrogen and oxygen at the respective surface sites by carrying out the required redox reactions. The feasibility of the redox reaction depends upon the energy of the electrons and holes generated in the SC due to absorption of photons. Hence, the catalyst should have both an appropriate band gap of $E_g > 1.23 \text{ eV}$ and suitable band edges saddling both the HER and OER potentials. An advantage of photocatalysis is that it directly uses the solar energy; thus there is no dependence on any other form of energy. However, very few catalysts fulfill the required band gap and band alignment criteria. It is even more difficult to find a catalyst composed of earth abundant low-cost elements with high absorption coefficients in the visible spectrum. Since the electrons and holes are not spatially separated as the hole and the electron are produced in the valence band (VB) and conduction band (CB) of the same material, the chances of recombination are very high. In the case of the PEC process, solar light is used as the primary source of energy; in addition to that a small electrical potential is applied essentially for the efficient separations of electrons and holes generated in the catalysis process. The application of a low bias

potential in PEC is the most important difference between photocatalysis and photoelectrocatalysis. In PEC, oxidation and reduction of water into oxygen and hydrogen occur at two different electrodes, viz., the photoanode and the photocathode, respectively, thereby decoupling the processes into two different locations of the PEC cell which allows different catalyst materials for fabrication of the respective electrodes. The process provides significant advantages, as the requirement of a large band gap as well as band edge position criteria is relaxed. Photoanodes should have valence band maxima more positive than the $\text{O}_2/\text{H}_2\text{O}$ potential, i.e., 1.23 V (in NHE scale), whereas the photocathodes should have conduction band minima more negative than the $\text{H}_2\text{O}/\text{H}_2$ potential, i.e., 0 V. The photoanode and photocathode can be optimized separately for the best possible efficiencies in terms of oxygen evolution and hydrogen evolution and ultimately be coupled to drive the overall water splitting process. The detrimental issue of the mixing of oxygen and hydrogen can be avoided in the PEC water splitting route.

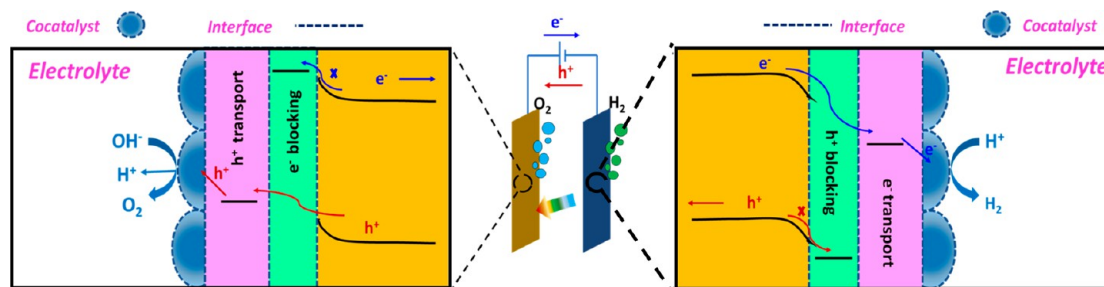
The mechanism of water splitting via the PEC route involves three steps:

- (i) generation of charge carriers by solar illumination on the photoelectrode
- (ii) transport of the charge carriers from the bulk of the semiconductor to the interface where it will be finally transferred to the electrolyte
- (iii) transfer of the charges to the electrolyte to carry out electrochemical oxidation or reduction of water

The schematic representation of the PEC water splitting process is shown in Scheme 2.

As the primary requirement the semiconductor should have a band gap above 1.23 eV. The energy losses due to the overpotential require additional energy, and a higher band gap is required. A higher side band gap of more than 3.2 eV is not recommended as it falls in the UV region and the solar spectrum has a significantly less proportion of the UV component. After the absorption of the solar light the generated charge carriers are to be transported for the charge transfer reaction at the interface; the material therefore requires good electrical conductivity. After transferring the charge up to the surface, it requires an efficient transfer to water; therefore, the charge transfer efficiency has to be good. The catalyst has to be stable for prolonged use to generate hydrogen and oxygen from water, especially in an environment where continuous generation of electrons and holes is taking place and these reactive electrons and holes have the capacity to degrade the catalysts. Finally, the catalyst should be generated from earth abundant material for sustainability. The issues with photoanodes and photocathodes are generally common; however, there are differences between the two processes as the oxygen evolution process is generally

Scheme 2. Schematic of the Photoelectrocatalytic Splitting of Water Using Photocathode and Photoanode



more complicated compared to the hydrogen evolution process. The present review discusses the improvement of the catalytic performances by rectification using material from crystal facet engineering and other surface modifications. The materials for efficient electrodes have been searched for, for several decades. The reports from Bard's group using scanning electrochemical microscopy (SECM) have proved SECM to be one of the important techniques to screen the compositions of photoelectrodes.³

The possibility of the use of HER and OER catalysts for the benchmarking of catalytic systems is carried out and reported in an important article. The catalytic systems with non-noble metal based catalytic systems that were summarized are based on Ni, Co, Mo, Fe, W, Cr, and Cu along with dopants like P, B, N, and S.⁴ The materials that fit well as photoanodes and have gained significant attention from researchers over the past two decades as low-cost, promising materials are TiO₂, α -Fe₂O₃, BiVO₄, CdS, group III–V semiconductors like InP, and GaAs. Cu₂O, CuBi₂O₄, transition metal sulfides, NiFeP, and layered double hydroxides (LDHs) have been identified as photocathodes.^{5–7} Several composite catalytic systems are also being designed to enhance the performances of both cathodic and anodic processes.^{4,8–12} The challenges with the catalytic systems include sustainability, which could be achieved through an efficient and stable catalytic system from earth abundant material. Some recent articles target the box strategies in generating materials, crystal orientations, and oxygen vacancy creation to overcome the difficulties in PEC catalysts.^{13–15}

There are reviews which discuss the materials and strategies to overcome the obstacles that come along the way of the sustainable generation of hydrogen from water through PEC routes. The elemental, chemical, structural, and orientational aspects of the materials suitable in PEC water splitting using solar light have been discussed.^{16–31} The terminologies that both the most while developing the efficient catalysts for PEC water splitting are fast electron–hole recombination, inefficient surface charge transfer, low conductivity of the material, photocorrosion, and catalytic systems generated from earth abundant elements. The present review has focused on the possibility to resolve the above-mentioned issues through the catalysts having orientational crystals, materials with suitable morphologies, treatments of the surfaces, and modulation of the surface electronic states.

2. REPRESENTATIVE PARAMETERS IN PHOTOELECTROCHEMICAL (PEC) MEASUREMENTS

When evaluating the performances of photoelectrochemical catalysts, the important parameters that were analyzed are presented below.

The separation of charges after their generation due to the photoexcitation is important in the catalysis process. The surface charge separation (η_{transfer}) and bulk charge separation ($\eta_{\text{transport}}$) efficiencies of photoelectrodes are the two important parameters in evaluating the efficiencies which are calculated using the following equations.

$$\eta_{\text{transfer}} = \frac{J_{\text{H}_2\text{O}}}{J_{\text{Na}_2\text{SO}_3}} \times 100\% \quad (5)$$

$$\eta_{\text{transport}} = \frac{J_{\text{Na}_2\text{SO}_3}}{J_{\text{max}}} \times 100\% \quad (6)$$

$$J_{\text{max}} = \frac{\text{integration of light absorption}}{\text{integration of solar light spectrum}} \quad (7)$$

where J_{max} is calculated from the photocurrent obtained from the silicon detector. $J_{\text{H}_2\text{O}}$ is photocurrent density of the water, and $J_{\text{Na}_2\text{SO}_3}$ is the photocurrent of the oxidation of the sulfite which is a hole scavenging agent (sacrificial agent) ensuring 100% utilization of the holes produced for the photoanodes. For the photocathode ethylene glycol, sodium sulfite, mixtures of sodium sulfide and sodium sulfite, glucose, and lactic acid are generally used as the sacrificial agents.^{17,20} There are efficiency parameters to evaluate the performance of the catalysis process. The incident photon to current efficiency (IPCE) is one of the important parameters, which is obtained by using the following equation:

$$\text{IPCE (\%)} = \left(\frac{J \left(\frac{\text{A}}{\text{cm}^2} \right) 1240}{P_{\text{in}} \left(\frac{\text{W}}{\text{cm}^2} \right) \lambda \text{ (nm)}} \right) \times 100\% \quad (8)$$

where J is the measured photocurrent density, P_{in} is the power of the incident monochromatic light (measured by the silicon-based detector), and λ is the wavelength in nanometers. IPCE represents the ratio of photon utilization, i.e., fraction of the photons which produces photocurrent to the total number of photons falling on the photoelectrode. IPCE does not account for the photons lost due to reflection or transmission without getting absorbed by the semiconductor photoelectrode. Rather, the absorbed photon to current conversion efficiency (APCE), which is derived from IPCE, is a better parameter to compare the photoanodes as it represents the ratio of the photons generating photocurrent to the total photons which are absorbed by the photoelectrode. It factors in the absorptivity of the photoelectrode in the visible region. APCE is calculated using the equation

$$\text{APCE (\%)} = \text{IPCE} / (1 - 10^{-\text{OD}}) \times 100\% \quad (9)$$

where OD is the absorbance of the material. The IPCE and APCE measurements provide sufficient information about the performance of the catalysis process. The calculation of IPCE and APCE depends essentially on the measured catalytic current; however, in the absence of the determination of the evolved hydrogen concentration from the catalysis process, these two parameters are well accepted in comparing the performances of the developed catalytic systems.

Finally, the solar to hydrogen efficiency (STH) defines the efficiency at which the PEC cell is able to generate hydrogen due to the exposure of one sun. The STH is defined as

$$\text{STH (\%)} = \left[\frac{\left(\frac{\text{mol of H}_2}{\text{s}} \right) \left(237000 \frac{\text{J}}{\text{mol}} \right)}{P_{\text{in}} \left(\frac{\text{W}}{\text{cm}^2} \right) A \text{ (cm}^2\text{)}} \right] \times 100\% \quad (10)$$

where the moles of hydrogen generated from the PEC process is normalized with respect to the energy deposited from the solar simulator. Another important term, applied bias photon to current efficiency (ABPE), is used when the experiments are carried out at a bias potential other than the redox potential of the water splitting process, i.e., 1.23 V. In this efficiency calculation the electrical energy equivalent to the bias potential has been subtracted.

$$\text{ABPE (\%)} = \frac{J_{\text{H}_2\text{O}}(1.23 - V_{\text{bias}})}{P_{\text{in}}} \times 100\% \quad (11)$$

The electronic property of the semiconductor is evaluated from Mott–Schottky measurements, where the experiments are performed at a fixed frequency with the variation of the applied bias potentials. The parameters like donor density (N_{D}) and flat band potential (V_{FB}) are determined from the plot of $1/C^2$ versus applied potentials in correlation with eq 12.

$$\frac{1}{C^2} = \frac{2}{qA^2\epsilon_0N_{\text{D}}}\left(V - V_{\text{FB}} - \frac{k_{\text{B}}T}{q}\right) \quad (12)$$

where C is the space charge capacitance, q is the elementary charge, A is the electrode surface area, ϵ_0 is the vacuum permittivity ($8.854 \times 10^{-12} \text{ F m}^{-1}$), ϵ is the relative permittivity of the photoanode, V is the applied potential, k_{B} is the Boltzmann constant ($1.38 \times 10^{-23} \text{ J K}^{-1}$), and T is the absolute temperature. The flat band potential (V_{FB}) indicates the extent of band bending; more band bending means more energy available for the minority carriers for the redox processes.

3. DISCUSSION ON THE ENHANCEMENT OF PERFORMANCE

On photoexcitation, charge carriers are generated at the surface of the semiconductor and also in the bulk of the material. Since the PEC processes happen at the electrode/electrolyte interface, the photogenerated charge carriers are required to be transported from the bulk of the semiconductor to the interface. Here, “the bulk of the semiconductor” means the entire thickness of the semiconductor film, which falls in the range from a few micrometers to about 100 μm . During the journey of photogenerated charge carriers from the bulk of the semiconductor to the semiconductor/electrolyte interface, the chance of recombination is very high and recombination is one of the primary reasons for the loss of catalytic efficiency and detrimental factors to achieving the targeted 10% solar to hydrogen (STH) conversion efficiency. The recombination of the charge carriers is categorized into two processes: bulk charge recombination and surface charge recombination. The recombination process in relation to the diffusion layer thickness of the charge carriers is reported with respect to the thickness of the catalyst used. The charge separation efficiency in BiVO_4 is reported to be better at a film thickness of about 458 nm; a separation efficiency of about 96% has been reported. Interestingly, the band gap property of BiVO_4 does not modify with the thickness of the film, which therefore indicates the important role of the charge carrier dynamics in the recombination process resulting in a higher catalytic efficiency.³² Bulk recombination can be reduced by modification of the crystal structure manipulation via doping, preferential growth of certain crystal facets, morphology optimization, etc., while the interfacial charge carrier recombination at the electrode/electrolyte interface can be managed via surface modifications, cocatalyst loading, and various postsynthetic treatments. Brief notes of the processes with a focus on the preferential generation of crystal planes and modification of the surfaces are discussed in the following sections.

3.1. Crystal Facet Engineering. The process of retardation of charge recombination through crystal facet engineering has evolved in the generation of the catalyst material with preferential orientation of the crystals. When a crystal grows from its nucleation state, the crystal facet with higher surface

energy grows faster and the crystal facet with lower surface energy grows slowly and thus dictates the shape of the crystal. This process leads to crystals with exposed facets of lower energy, whose reactivity is rather lower than that of the high energy facets, which are relatively less useful in solar energy conversion. The crystal facet engineering is essentially generated from the preferential arrangement of the atoms in a particular direction. Anisotropy can be exploited for the synthesis of photoelectrodes for better efficiency. Examples of three major sources of anisotropy—electronic anisotropy, surface built-in electric field, and electrical conductivity—responsible for the modifications of the catalytic properties are discussed in brief.

Electronic anisotropy has been observed in WO_3 , an important photoanode; the material has a band gap in the wide range of 2.75–3.25 eV. When a WO_3 crystal has equally exposed {002}, {020}, and {200} facets, the crystal is named QC- WO_3 and the observed band gap is 2.71 eV, while for the exposure of the {002} plane the crystal is named RS- WO_3 and shows a band gap of 2.79 eV. Further, the VB and CB are elevated by 0.22 and 0.30 eV respectively in the case of the {200} exposed RS- WO_3 crystal with respect to QC- WO_3 . Excluding the effect of surface area, normalized oxygen evolution has been reported 8-fold higher in QC- WO_3 than in RS- WO_3 .³³ The modulation of the electronic properties in relation to the crystal facet engineering has been explored in several other materials.^{34–43} The dynamics of the photogenerated electrons are highly affected by the exposed facet. In anatase TiO_2 , the {101} and {001} facets behave differently toward electron and holes in aqueous solution. Excess electrons at aqueous {101} facets favored the reduction of water at {101} facets, while {001} facets attract holes and strongly repel electrons, thereby favoring oxidation.⁴⁴

The spatially resolved surface photovoltage spectroscopy (SRSPS) technique has enabled researchers to understand the generation of surface photovoltage (SPV), an important facet dependent property. Different SPVs on different facets indicate differences in band bending on respective facets, leading to built-in electric fields which facilitate separation of electron–hole pairs into favored facets, thereby reducing the recombination. Such properties are observed with the well-investigated photoanode BiVO_4 . The driving force for the interfacet charge separation between {011} and {010} facets is only 3.8 mV, as the upward band bending is approximately 7.2 and 3.4 mV on the {011} and {010} facets, respectively. This will lead to the transport of holes to the {011} facet and electrons to the {010} facet. The resultant driving force can further be enhanced by selective deposition of cocatalysts on the facets. In another investigation, the selective deposition of MnO_x on the {011} facet and Pt on the {010} facet enhances the driving force to 174 mV. Thus, the selective transport of holes and electrons to different facets generated the facet dependent redox reactions which resulted in the modification in the surface catalytic properties and enhancement in the performance.⁴⁵

The surface charge is tuned through the fluorination of BiVO_4 photoanode surfaces. The surface treatments by fluorination have been proved to be good in enhancing the OER process.^{46–48} The fluoride anion has an ionic radius similar to that of oxygen, but it has higher electronegativity. The fluoride ion could replace the O ions at the surface and generate metal–fluoride bonds at the surface. The metal–fluoride bond enhances the conductivity of the material; the highly polar metal–fluoride bond at the surface essentially regulates the adsorption property during the OER process and enhances the

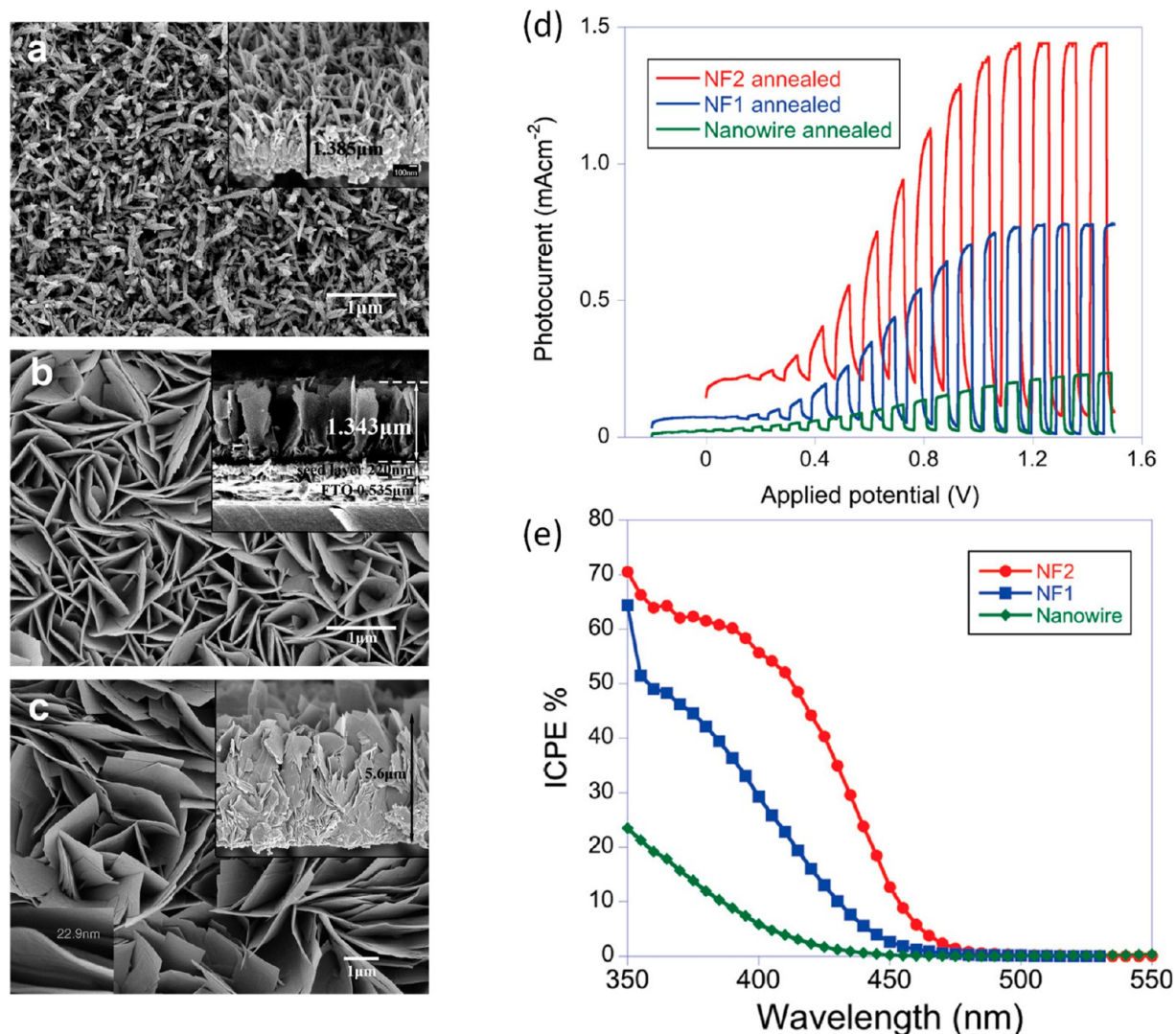


Figure 1. FESEM images of unannealed WO_3 : (a) nanowire, (b) NF1, and (c) NF2 arrays. Insets show film cross section. (d) Current–potential plots for WO_3 photoanode annealed nanowire and two flake samples (NF1 and NF2), under chopped visible light in an aqueous solution of 0.1 mol/L sodium sulfate (Na_2SO_4). (e) IPCE of three samples. Reprinted from ref 60. Copyright 2011 American Chemical Society.

catalytic performance. In an additional mechanistic investigation, the photogenerated holes at the bulk of the material have enhanced driving force to be transported toward the surface of the catalysts having more polar metal–fluoride bonds. Such enhanced transfer of holes would increase the electron–hole charge separation, and thus the catalytic performance has been reported to be enhanced by almost 100%.⁴⁹

In symmetric crystals like octahedrons and nanocubes with no preferred direction for carrier transport, electrical conductivity varies when measured along a particular direction. In the Cu_2O octahedron, where the faces are bound by $\{111\}$ facets, electrical conductivity is 1100 times higher than that of the nanocubes where faces are bound by $\{100\}$ facets.⁵⁰ A similar observation is reported for hematite ($\alpha\text{-Fe}_2\text{O}_3$) photoanodes where conductivity along the $\{110\}$ direction is 4-fold higher than along the orthogonal direction.⁵¹ Hence, the synthesis of photoelectrodes with preferred facets facilitates desired oxidation or reduction reactions due to directional conductivity. The homojunction of the $\{001\}$ and $\{110\}$ planes has proved to enhance the PEC catalytic performance of the BiVO_4 system. The crystal facets have enhanced the charge transfer dynamics and also decreased the Gibbs free energy of water oxidation;

thus, the photocatalytic efficiency has been enhanced. The homojunction formation of nanodots of BiVO_4 and the wormlike morphology of BiVO_4 proved to be good in the overall PEC performance of water oxidation.⁵² Higher electronic conductivity has been reported in the (0001) basal plane of single crystalline $\alpha\text{-Fe}_2\text{O}_3$. The catalytic system is reported to be stable; the developed catalysis system has lowered the charge recombination and enhanced the charge transfer resistance, which resulted in the enhancement in the PEC performance.⁵³

3.2. Modulation of the Surface Morphology. Along with the crystal facet engineering, the optimization of the morphology of the photoanode surface is important in deciding the PEC catalytic performance. The average lifetime and the mean diffusion length of any material is intrinsic to the material, but manipulation of the morphology can reduce the recombination and thus enhance the diffusion length of the charge carrier. Moreover, the engineered surface morphology enhances the effective surface area of the photoelectrode, increases the number of catalytic sites on the surface, accelerates interfacial charge transfer, enhances light absorption, and reduces charge carrier trapped surface states.^{54–59} Important investigations and reports are available on surface morphology

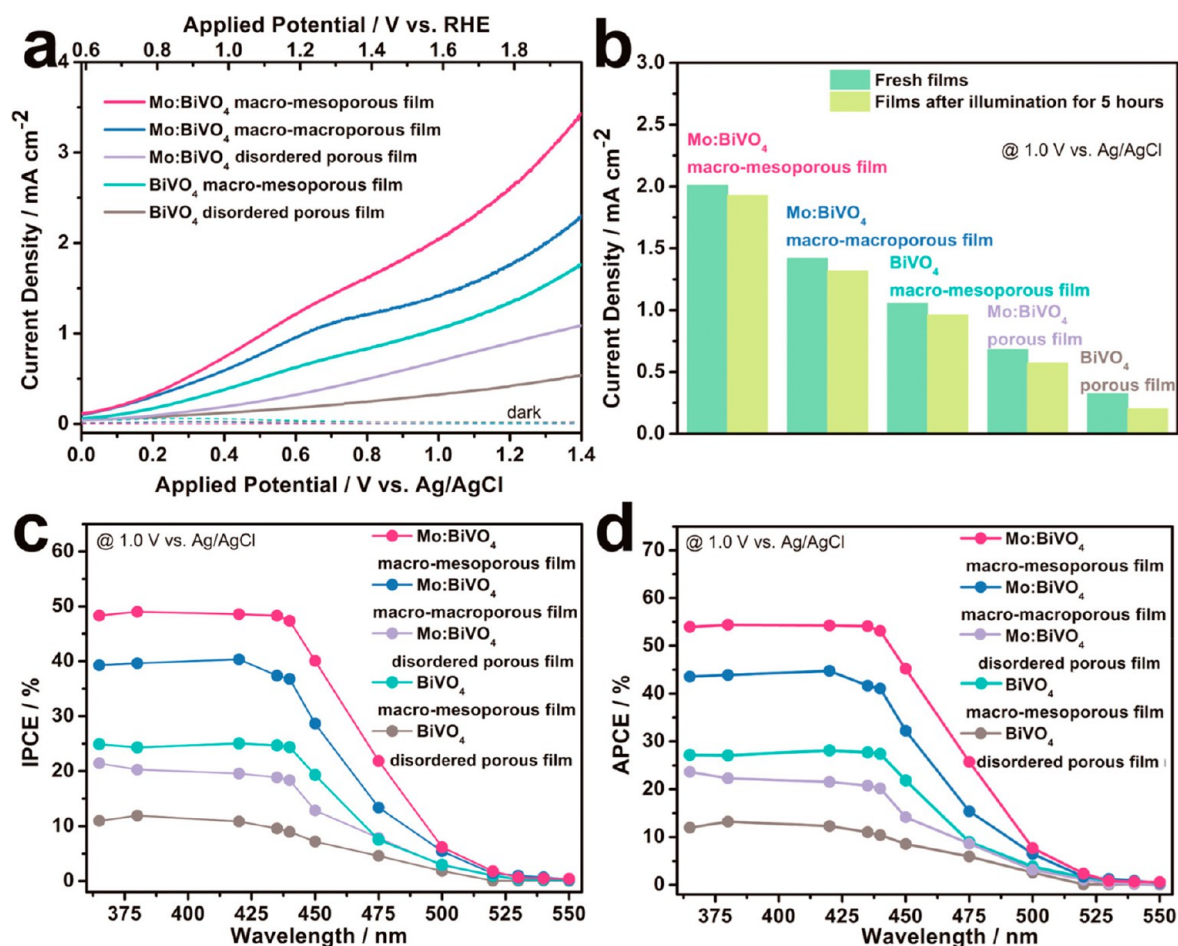


Figure 2. (a) Photocurrent density–potential curves (solid lines) and dark current density–potential curves (dashed lines) of various films (scan rate = 10 mV s⁻¹). (b) Stability of the photocurrent density of various films at 1.0 V vs Ag/AgCl. The films for measurement are fresh and after illumination for 5 h, respectively. (c, d) IPCEs and APCEs of various films as a function of the wavelength at 1.0 V vs Ag/AgCl. Reprinted from ref 61. Copyright 2014 American Chemical Society.

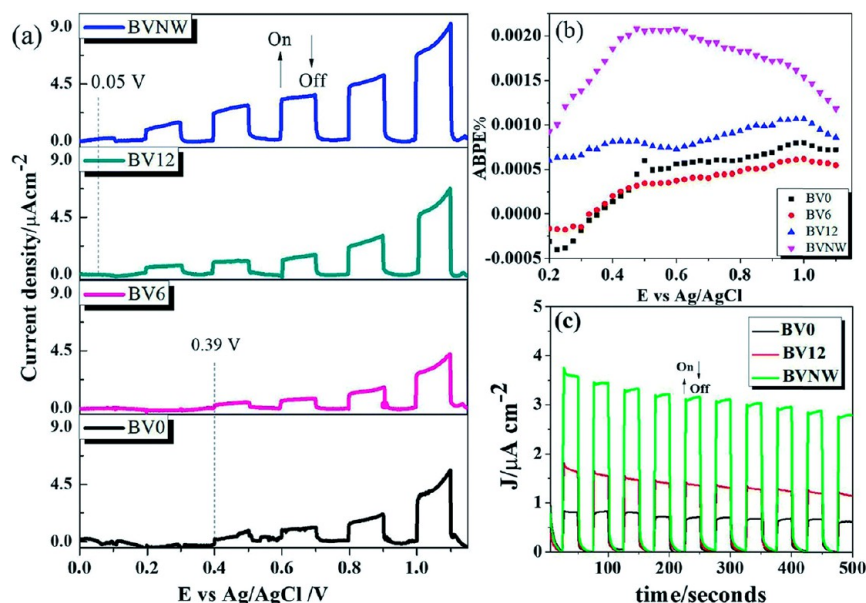
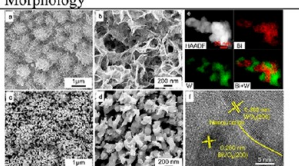
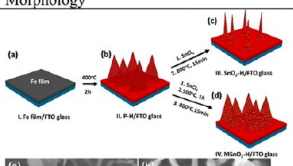
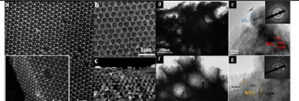
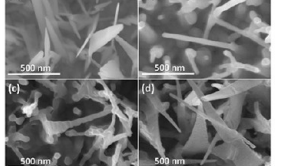
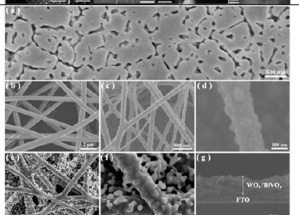
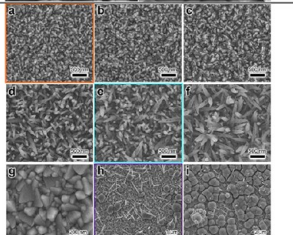
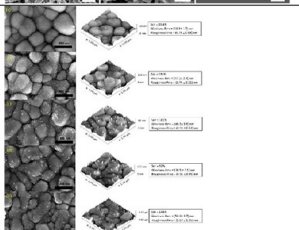
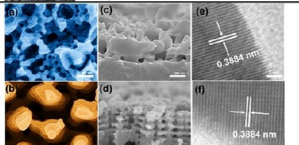
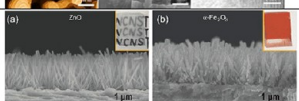
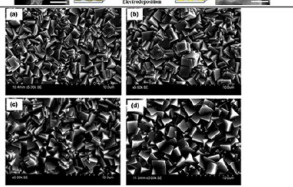


Figure 3. (a) Linear sweep voltammograms of BiVO₄ electrodes measured in 0.5 M phosphate buffer at a scan rate of 5 mV s⁻¹ under 1.5 G simulated solar light under chopped light conditions, (b) Corresponding applied bias photon-to-current efficiency (ABPE%) for various BiVO₄ photoanodes. (c) Amperometric photocurrent–time profile for various BiVO₄ photoelectrodes under the same simulated light, also under chopped light (on/off) conditions and at a bias of 0.6 V vs Ag/AgCl. Reprinted with permission from ref 62. Copyright 2019 Royal Society of Chemistry.

Table 1. Morphologies of Materials and Resulting Current Density Values⁴

Electrode	Morphology	Performance	Ref	Electrode	Morphology	Performance	Ref
Hierarchical WO ₃ /BiVO ₄		Hierarchical WO ₃ /BiVO ₄ 6 mA cm ⁻² at 1.23 V vs RHE, while the flat WO ₃ /BiVO ₄ 3.4 mA cm ⁻²	[65]	Hematite		P-H: 0.38 mA cm ⁻² Sn-H 0.63 mA cm ⁻² SnO ₂ -H : 0.92 mA cm ⁻² MSnO ₂ -H : 1.08 mA cm ⁻² at 1.50 VRHE	[69]
Three-Dimensional FTO/TiO ₂ /BiVO ₄ inverse opal morphology		4.11 mA cm ⁻² at 1.23 V	[63]	Fe ₂ O ₃ nanocoral and Fe ₂ O ₃ nanorod		Fe ₂ O ₃ -nc-100 min: 0.61 mA cm ⁻² at 1.23 V vs. RHE Fe ₂ O ₃ -nr-195 min: 1.19 mA cm ⁻² at 1.23 V vs. RHE	[70]
FTO/ID-WO ₃ /BiVO ₄		2.8 mA cm ⁻² (at 1.23 V vs. RHE)	[64]	BiVO ₄		Pristine BVO: 1.09 mA cm ⁻² BCF-H: 2.64 mA cm ⁻² BCCF-H: 3.91 mA cm ⁻² at 1.23 V vs RHE	[71]
TiO ₂ films		0.13 mA cm ⁻² unmodified 0.26 mA cm ⁻² Modified (at 1.23 V vs. RHE)	[66]	WO ₃		3.0 mA cm ⁻² at 1.23 VRHE, increasing by 151% compared to that of PW (1.19 mA cm ⁻²)	[67]
Hematite		Polycrystalline Hematite ~0.23 mA cm ⁻² vs single crystalline hematite ~0.69 mA cm ⁻² at 1.23 V RHE	[68]	ITO/BiNP _{film} /Cu ₂ O, ITO/BiNP _{sus} /Cu ₂ O, ITO/Bi _{ion} /Cu ₂ O, and ITO/Cu ₂ O		ITO/BiNP _{film} /Cu ₂ O: 5.2 mA cm ⁻² , ITO/BiNP _{sus} /Cu ₂ O, 4.9 mA cm ⁻² , ITO/Bi _{ion} /Cu ₂ O, 3.7 mA cm ⁻² and ITO/Cu ₂ O 2.6 mA cm ⁻²	[72]

⁴Including figures reprinted as follows: Reprinted from ref 63. Copyright 2017 American Chemical Society. Reprinted with permission from ref 64. Copyright 2018 Elsevier B.V. Reprinted from ref 65. Copyright 2017 American Chemical Society. Reprinted from ref 66. Copyright 2015 American Chemical Society. Reprinted from ref 67. Copyright 2023 American Chemical Society. Reprinted with permission from ref 68. Copyright 2023 Elsevier B.V. Reprinted from ref 69. Copyright 2022 American Chemical Society. Reprinted with permission from ref 70. Copyright 2023 Elsevier B.V. Reprinted with permission from ref 71. Copyright 2019 Wiley. Reprinted with permission from ref 72. Copyright 2016 Royal Society of Chemistry.

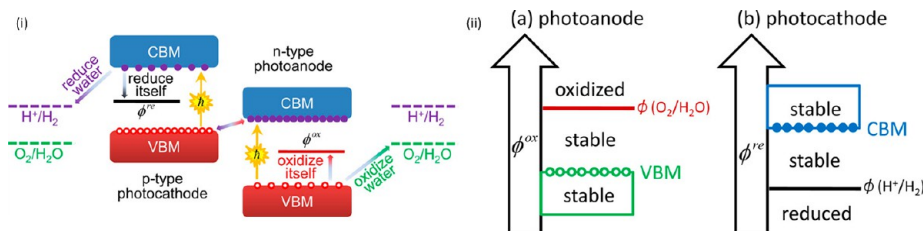
dictated improvements in the photocurrent generation efficiency. Su et al.⁶⁰ synthesized WO₃ photoanodes with both nanowire and nanoflake morphologies through the solvothermal method; the results are shown in Figure 1. The nanoflake morphologies named NF1 and NF2 resulted in higher PEC performance; 60% more IPCE with a photocurrent density of 1.43 mA cm⁻² at 1.23 V vs NHE compared to nanowire morphology has been reported.⁶⁰

Disorder in the geometrical structure effectively increases the distance traveled by charge carriers before the reaction and thus reduces the collection efficiency. Long-range-ordered paths provided by interconnected periodic microporous structures facilitate electron transport throughout the electrodes and improve the hole utilization. Zhou et al.⁶¹ have designed an inverse opal-type BiVO₄ photoanode with ordered microporous and mesoporous structures along with disordered porous film. The results of the PEC efficiency obtained from the chopped

light voltammetry and IPCE/APCE measurements are shown in Figure 2. The ordered films showed significant improvement in the photocurrent density along with a higher IPCE. From the decay kinetics of the photocurrent transient, the transient time constant (τ) can be extracted; a higher value of τ indicates lower recombination. The value of τ increases from 1.1 to 3.0 s when the geometric structure is transformed from the disordered structure to the ordered structure, respectively.⁶¹

Dey et al.⁶² have optimized the nanoworm morphology of BiVO₄ for water splitting and regulated the morphology by tuning the time of hydrothermal reaction during the synthesis process. The materials named BVX (where X = time of hydrothermal reaction in hours) show improved photocurrent density when the time of reaction is 18 h, leading to nanoworm morphology compared to the nanowire morphology formed via 12 h of reaction, shown in Figure 3. The values of τ obtained from the transient photocurrent decay plot remain 3.42 s for

Scheme 3. (i) Schematic Plot of the Band Alignment of p-Type Photocathode and n-Type Photoanode Semiconductors Relative to the Water Redox Potentials in the Z-Scheme;^a (ii) Stability Change of the Photoanode (a) as Its Oxidation Potential ϕ_{ox} Shifts Up from below the VBM to above $\phi(\text{O}_2/\text{H}_2\text{O})$ and of the Photocathode (b) as Its Reduction Potential ϕ_{re} Shifts Down from above the CBM to below $\phi(\text{H}^+/\text{H}_2)$ ^b



^a ϕ_{ox} shows the oxidation potential of the photoanode in aqueous solution, and ϕ_{re} shows the reduction potential of the photocathode. ^bReprinted from ref 73. Copyright 2012 American Chemical Society.

BV18 and 8.49 s for BV12, implying a rather suppressed charge carrier recombination, which is further supported by a larger space charge region width in the case of the former leading to sharper band bending which in turn improves the charge separation.⁶²

Modulated surface morphology can also be used to improve the quality of the heterojunction layer, which will finally enhance the overall efficiency of the photoelectrode. To improve the electron extraction at the back contact of the photoanode, generally an n-type semiconductor having a long electron diffusion length is used as the heterojunction layer. Since the diffusion length of the charge carrier in the actual photoanode layer is low, a porous or one-dimensional heterojunction layer decorated with a photoanode layer is advantageous, as the effective distance traveled by the charge carriers inside the photoelectrode is less. The inverse opal heterojunction layer of TiO_2 on FTO and BiVO_4 layer prepared by Zhang et al.⁶³ shows a current density of 0.94 mA cm^{-2} compared to 0.48 mA cm^{-2} in bare BiVO_4 . The τ obtained for FTO/ TiO_2 / BiVO_4 (7.4 s) is longer than that of FTO/ BiVO_4 (3.9 s), indicating significant suppression in e–h recombination.⁶³ Xu et al.⁶⁴ prepared FTO/1D WO_3 / BiVO_4 photoanodes via the electrospinning method. The FTO/1D WO_3 / BiVO_4 showed a photocurrent density of 2.8 mA cm^{-2} at 1.23 V vs RHE, which is twice that of FTO/ BiVO_4 (i.e., 1.56 mA cm^{-2} at 1.23 V vs RHE). Such an improvement has rooted through the better charge carrier separation and charge transport which has been indicated by detailed investigations using several complementing techniques.⁶⁴

Materials with different surface morphologies along with the generated current density parameter are summarized in Table 1. Crystal facet engineering and surface morphology tailoring are very crucial for charge carrier generation and transport of the same to the electrode/electrolyte interface.

However, because water oxidation kinetics is an exceptionally slow process, achieving the effective utilization of holes is not an easy task. Photogenerated charge carriers after reaching the electrode/electrolyte interface indulge in several other side reactions, most of which lead to corrosion of the photoanode itself. Hence, effective surface modification to facilitate charge transfer from the electrode to the electrolyte or for protection against photocorrosion should be introduced. The process includes protective layer coating, cocatalyst loading, and postsynthetic modification for reduction of charge carrier trapping surface states; brief notes about such processes are discussed in the following sections.

3.3. Protective Layer Coating and Surface Electronic States. Apart from the basic requirement of band alignment, i.e., valence band maxima (VBM) lying at lower potential than $E(\text{O}_2/\text{H}_2\text{O})$ for an n-type semiconductor and conduction band maxima (CBM) lying higher than $E(\text{H}_2\text{O}/\text{H}_2)$, alignment of the energy levels of the photogenerated charge carriers with respect to water oxidation and reduction potentials and the self-reduction (Φ_{red}) and self-oxidation (Φ_{ox}) potentials of the semiconductor is also crucial. As has been mentioned, the long-term stability of the photoelectrode is one of the most desired characteristics for practical application of the PEC process. The self-oxidation and self-reduction of the catalysts have been the most detrimental factors in reducing the stability of the photoelectrodes. The kinetically sluggish water oxidation makes the competitive consumption of the photogenerated charge carriers and the side reactions, which in most events corrode the electrode material itself leading to instability and gradual deterioration in performance. The process in PEC literature is termed “photocorrosion”. The stability of a photoelectrode under operating conditions depends upon its relative Φ_{red} and Φ_{ox} with respect to $E(\text{H}_2\text{O}/\text{H}_2)$ and $E(\text{O}_2/\text{H}_2\text{O})$, respectively, which has been presented schematically in Scheme 3. A material will become thermodynamically unstable if Φ_{red} is placed below $E(\text{H}_2\text{O}/\text{H}_2)$ or if Φ_{ox} is above $E(\text{O}_2/\text{H}_2\text{O})$.

Apart from the photocorrosion, dissolution of metal ions in the aqueous solution without any change in the oxidation state also leads to deterioration of the photoelectrodes due to loss of the photoactive layer. Hence, protection of the photoelectrode from these processes is only possible by coating a thin layer with suitable self-reduction (Φ_{red}) and self-oxidation (Φ_{ox}) potentials and preferably resistant to dissolution.^{28,73–75} In addition to its original role of surface passivation and to improve chemical and PEC stabilities under operating conditions, the passivating layers are designed to enhance the PEC performance by preventing the formation of deleterious surface states which act as centers for e–h recombination. The relative shifting of band position and favorable surface charge distribution enhances the catalytic performance of the water oxidation kinetics.

Semiconductor photoelectrodes are polycrystalline. Inherently they have more grain boundaries and surface defects, which favors recombination of photogenerated charges. In such cases surface passivation layers help in passivating these detrimental surface states. Passivation layers can also alter the onset potential of a catalyst electrode. The onset potential of the anode is defined by the following equations:

$$V_{\text{on,A}} = E(\text{A}^-/\text{A}) - V_{\text{ph}} + \eta \quad (13)$$

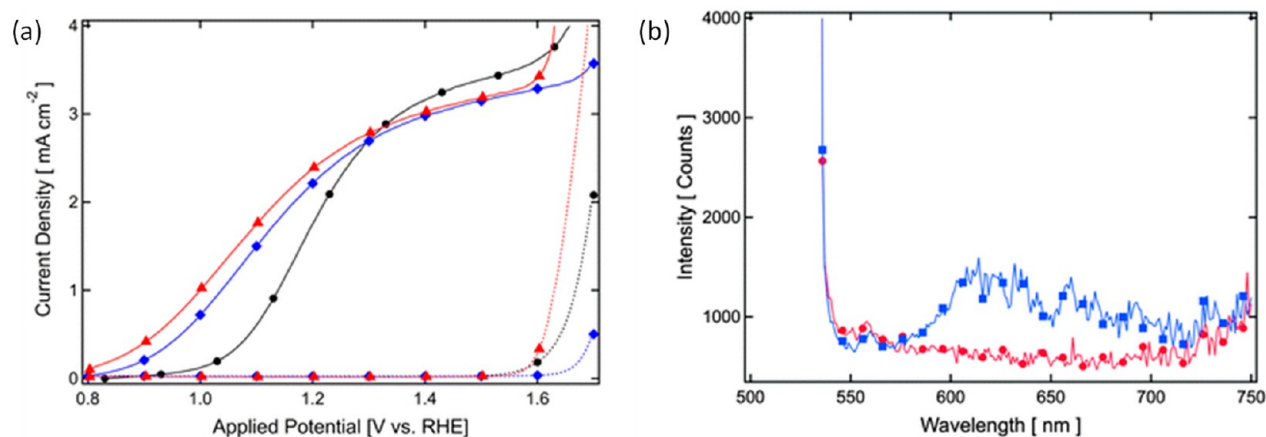


Figure 4. (a) Current densities, in mA cm⁻², of the prepared photoanodes in the dark (broken lines) and under simulated solar illumination (AM 1.5G 100 mW cm⁻², solid curves) shown as a function of the applied potential, V vs RHE. A hematite photoanode has been characterized before ALD treatment (black circles), after three ALD cycles of alumina and annealed to 400 °C (blue diamonds) and after subsequent cobalt treatment (red triangles). (b) Photoluminescence emission spectra (excitation wavelength = 520 nm) of a hematite cauliflower-type nanostructure photoanode before (red circles) and after three ALD cycles of Al₂O₃, on its surface (blue squares). Reprinted from ref 85. Copyright 2011 Royal Society of Chemistry.

$$\Delta V = E(A^-/A) - V_{\text{on},A} = V_{\text{ph}} - \eta \quad (14)$$

where $V_{\text{on},A}$ is the onset potential, $E(A^-/A)$ is the redox pair potential, V_{ph} is the photovoltage, and η is the kinetic overpotential. For a fixed redox pair, ΔV relates to the photovoltage without any kinetic overpotential loss, i.e., analogous to open circuit voltage. Surface passivation layers can modulate the surface environment, which reduces either the catalytic overpotential or surface recombination, leading to increased photovoltage, signifying greater band bending as well as a cathodic shift in the onset potential. The thin films of wide band gap semiconductors like Al₂O₃, Ga₂O₃, TiO₂, CoO_x, ZnFe₂O₄, and NiO_x coated over the photoelectrodes are generally better suited for the surface passivation layers.^{76–81}

The generation of ultrathin surface films using the atomic layer deposition (ALD) technique has been highly popular. It has been introduced for surface coating in PEC water splitting, essentially to reduce the photocorrosion of the catalyst substrates. The capability of the generation of ultrathin films using ALD with increments in the scale of nanometers does not modify the light absorption properties of the catalysts.^{82–84} Investigations further suggest that the ultrathin films of Al₂O₃ and TiO₂ have several important roles, like the modulation of surface states and the formation of favorable intermediates due to the surface diffusion of Ti or Al from the thin films to the bulk of the material.

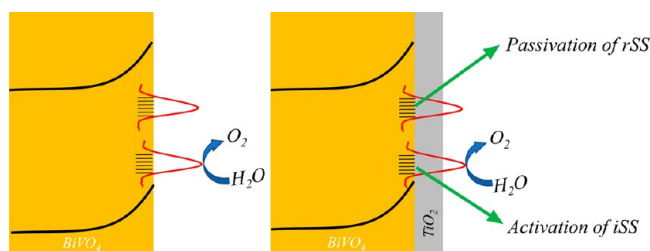
The enhancement of the charge transfer efficiency has been reported through the generation of surface defects. Surface defects are generated by chemical treatments or by laser or plasma treatments of the surfaces. The surface defects also act as the adsorption centers of reactive species. However, at higher defect concentrations the defects might act as the centers of charge recombination, which is detrimental to the PEC performance.⁵⁹

Hematite photoanode is very promising in terms of fulfilling the requirements of the band gap (2.1 eV), allowing it to absorb a significant portion of the solar spectrum. However, the surface trap states limit the performance by acting as centers for electron–hole (e–h) recombination and are also responsible for high overpotentials. Hence, in applying thin passivation layers of various materials, the surface trap state density can be modulated to improve the performance. Le Formal et al. applied ALD-

Al₂O₃ for reduction in the overpotential of Fe₂O₃ photoanode by 100 mV and enhanced the current density by 350% at 1 V vs RHE.⁸⁵ ALD-Al₂O₃ was able to passivate the surface states and reduce the accumulation of charges at the semiconductor liquid junction. More compelling evidence was obtained from photoluminescence spectra. Photoluminescence in solid state materials is heavily dependent on trapping of the surface states' density, as they provide a nonradiative recombination pathway for the photogenerated excitons. Thus, even partial elimination of these surface states results in enhanced photoluminescence, indicating lesser recombination of e–h. The enhancement in the photoluminescence property due to the elimination of the surface states due to the ALD-Al₂O₃ surface layer is shown in Figure 4.

Wong and co-workers⁸⁶ have also reported the improvement in the catalytic performance of hematite photoanodes using an ALD-TiO₂ outer layer. The samples were subjected to the annealing process at different temperatures; the heat treated ALD-TiO₂ thin films have a superior effect on the enhancement in the PEC catalytic process. The formation of surface defects has been revealed on the heat treated ALD-TiO₂ containing samples, which has a beneficial effect on the enhancement in the catalytic efficiency. The surface state mediated charge transfer has been discussed regarding the enhancement in the PEC efficiency. The charge transfer resistance from the surface trap states are deconvoluted from impedance measurements; the charge transfer resistance of the surface states is reported to be decreased on the annealed ALD-TiO₂ samples.⁸⁶ Recent work on the surface state passivation by Sharma et al.⁸⁷ shows the effect of modulation of surface states by ALD-TiO₂ on a BiVO₄ photoanode. In parallel to surface state passivation, TiO₂ improves the photocurrent density and onset potential. Intensity modulated photocurrent spectroscopy (IMPS) has been used by the researchers to evaluate the charge transfer and charge carrier recombination kinetics of bare and protected photoanodes. Moreover, the specific role of TiO₂ in modulating specific types of surface state has been investigated. The related results are represented in Scheme 4. Two types of surface electronic states are generally discussed when explaining the charge transfer processes at the photoanode and the solution interface. The recombining surface states (r-SS) are essentially responsible for enhancing the charge recombination process, a detrimental

Scheme 4. Depiction of the Modulation of Surface States Due to ALD-TiO₂ Thin Films at the Surface of BiVO₄^{4a}



^aReprinted from ref 87. Copyright 2023 American Chemical Society.

process for an efficient catalyst. The intermediate surface states (i-SS) are responsible for efficient charge transfers. Charge transfer and recombination rate constants obtained by modeling the IMPS data suggest improvement in the charge transfer. The surface modifications by the ALD-TiO₂ layer has a positive impact in enhancing the density of the i-SS which enhances the photoelectrochemical oxidation of water in addition to the protective role of the TiO₂ outer layer formed through ALD deposition.⁸⁷

In addition to TiO₂, the ultrathin outer layer of Al₂O₃ by ALD over the BiVO₄ surface has been investigated. The ultrathin Al₂O₃ films have an impact on the retardation of the electron and hole; however, the kinetics of the water oxidation process remain unaltered. The proposition on the modulation of surface states and its consequent enhancement in the water oxidation kinetics for ALD-Al₂O₃ modification of BiVO₄ is not supported from this report.⁷⁶ The surface passivation layer, which does not have an active role in the improvement of kinetics of water oxidation, will act only as a physical barrier between the photoactive layer and the electrolyte. The surface passivation layer with a chemical composition such that it can effectively relay the charge carrier between the photoactive layer and electrolyte acts as cocatalyst by acting as a center for charge transfer. Hence, it reduces the activation energy for the water oxidation/reduction process and enhances the efficiency and the stability.

3.4. Enhancement of PEC Efficiency by Cocatalyst Loading at the Surface. As discussed earlier, the oxygen evolution reaction is kinetically sluggish, which limits the STH efficiency. Cocatalysts act as centers of charge transfer between the photogenerated charge carriers and adsorbed H⁺ and OH⁻ ions for the reduction/oxidation of water. They selectively

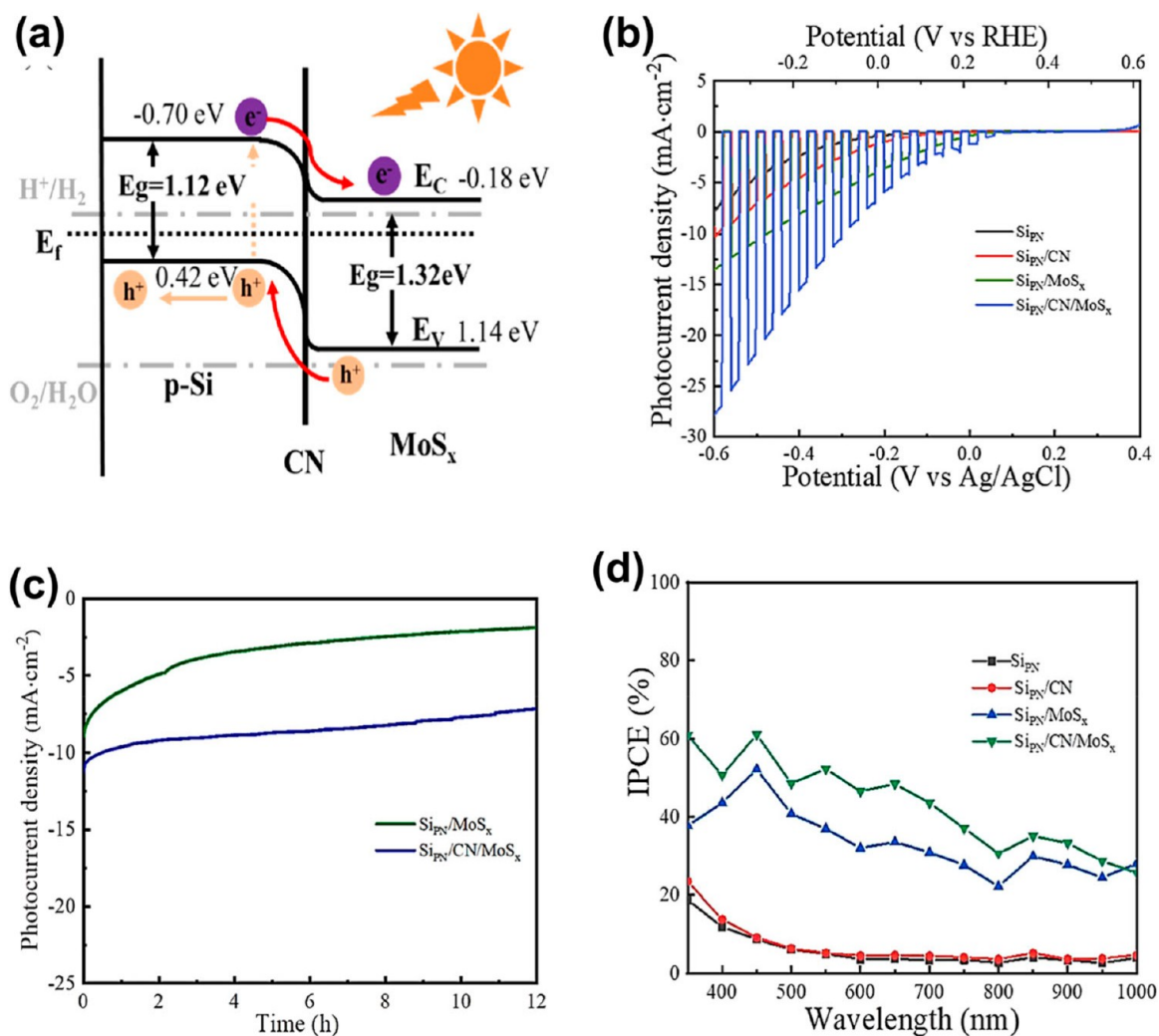


Figure 5. p-Si/CN/MoS_x photocathode for PEC water splitting. (a) Schematic representation of the p-Si/CN/MoS_x band structure diagram. (b) LSV curves showing the PEC performance under chopped illumination. (c) Chronoamperogram curves of the photocathodes. (d) IPCE measurement of the photocathodes. Reprinted from ref 92. Copyright 2022 Elsevier B.V.

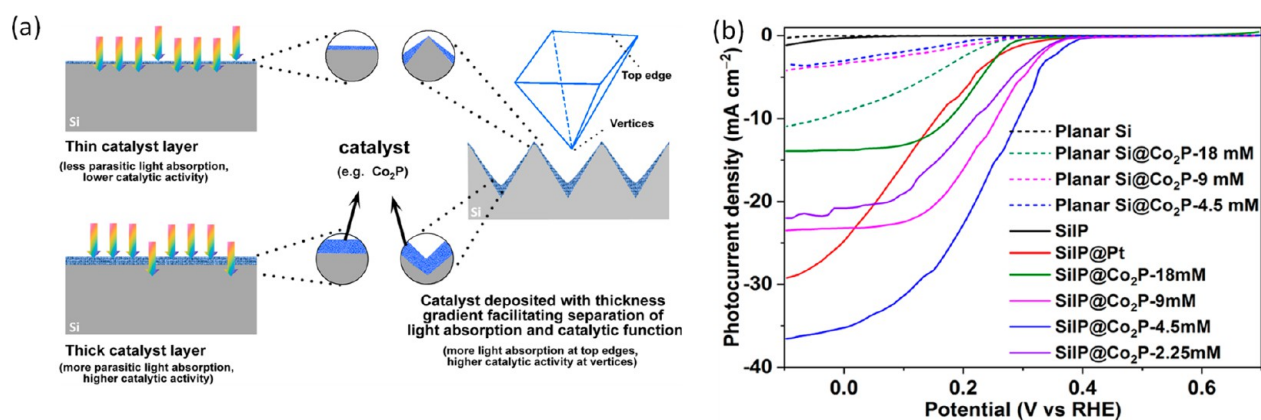


Figure 6. (a) Schematic illustration of the influence of catalyst loading on the light absorption of semiconductor photoelectrodes and the advantages of the SiIP configuration with a thickness-gradient catalytic/protective layer. (b) PEC performance of SiIP@Co₂P and planar Si@Co₂P photocathodes measured in 0.5 M H₂SO₄ under AM 1.5G illumination. Reprinted from ref 97. Copyright 2019 American Chemical Society.

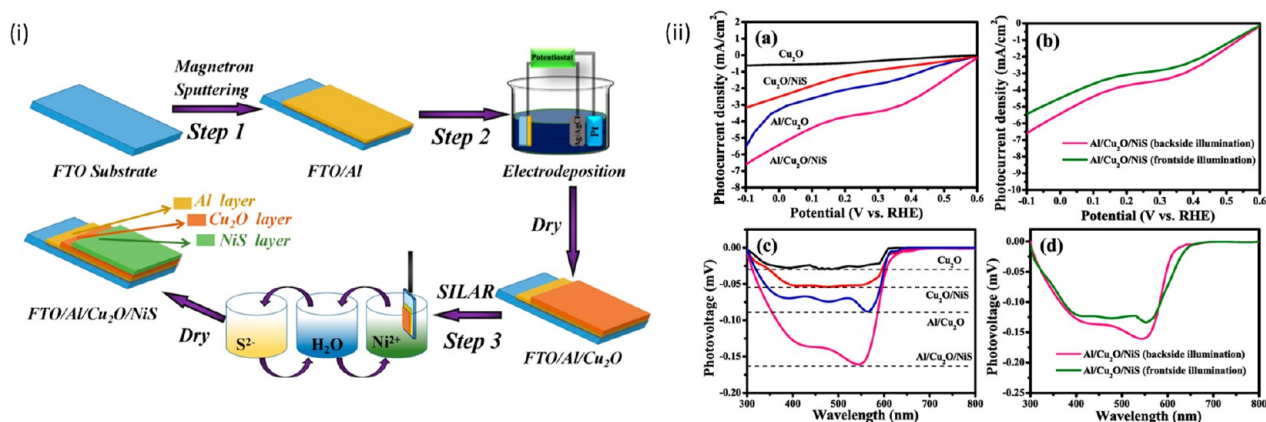


Figure 7. (i) Schematic illustration of the synthesis procedure of FTO/Al/Cu₂O/NiS photocathode. (ii) (a and b) Photocurrent density–voltage curves in 0.1 M Na₂SO₄ solution and (c and d) surface photovoltage spectroscopy irradiated from the back side of the samples. Reprinted from ref 98. Copyright 2020 Elsevier B.V.

enhance the surface kinetics by acting as traps for photo-generated charge carriers and extract them more effectively than bare photoelectrodes. Also, a highly active and large surface area provides more adsorption sites for H⁺ and OH⁻, which are involved in the reduction/oxidation of water. Resistance to charge buildup and quick utilization of the photogenerated e–h pair significantly enhance kinetics and reduce photocorrosion.^{28,88–91} Cocatalyst alters the reaction coordinate by providing a low activation energy pathway and thereby facilitating the complex four electron transfer process. IrO₂, RuO₂, and Pt are among the known noble metal catalysts, while MoO_x, MoS₂, CoB_y, CoP_z, FeOOH, NiOOH, and transition metal layered double hydroxides are examples of a few cost-effective earth abundant cocatalysts for photoanodes which have good efficiency and stability for PEC water splitting.

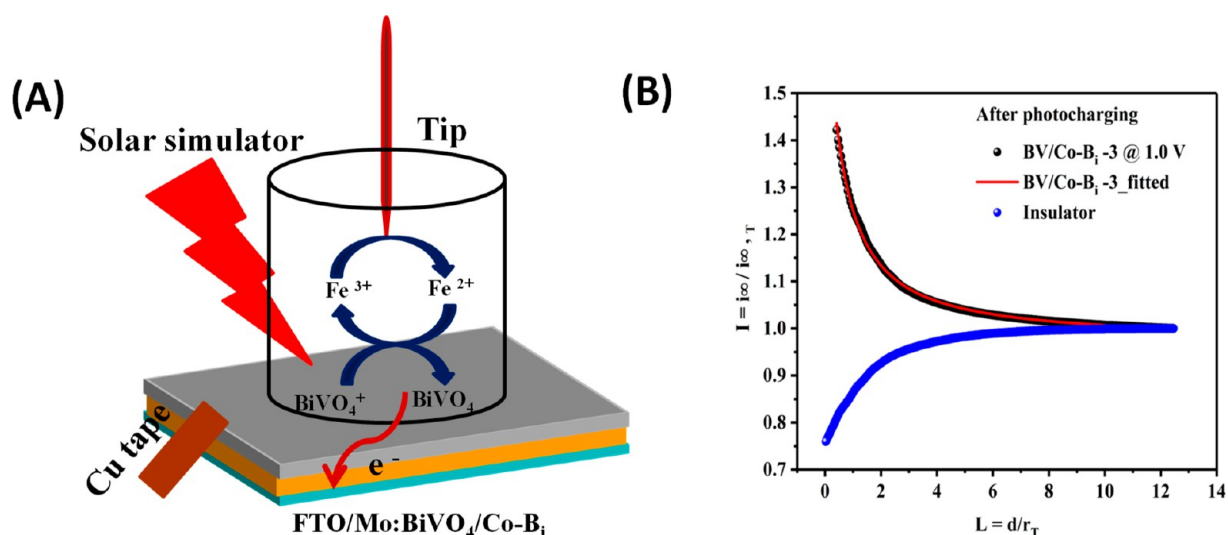
MoS₂ is a well-known electrocatalyst for HER, which has been widely applied by researchers as a cocatalyst for several photocathodes. Zhang et al.⁹² synthesized Si_{pN}/CN/MoS_x, where p–n junction Si substrate was used to facilitate outward migration of the photogenerated charge carriers due to an in-built buried junction and N doped carbon (CN) was inserted to improve electron conductivity, while MoS_x was coated on the top by photoassisted electrodeposition to improve the charge transfer behavior of the photocathode. The photocurrent density of Si_{pN}/CN/MoS_x at 0 V vs RHE is 6.5 times higher

than that of Si_{pN}/MoS_x. IPCE also improves significantly due to the high charge transfer efficiency at the electrode/electrolyte interface. Due to lesser accumulation of electrons at the interface, the stability against photocorrosion enhances, which is clearly evident from the *J*–*t* curve (cf. Figure 5c) showing lesser deterioration in photocurrent density over time.⁹²

The thickness of the cocatalyst becomes a limiting factor in such cases. A thicker layer of the cocatalyst would result in higher parasitic absorption and reflective losses, while a thinner cocatalyst layer would compromise PEC efficiency.^{93–96} Thalluri et al.⁹⁷ have discussed this problem by morphology engineering of the substrate which also acts as the protective coating. Inverted pyramid p-Si wafers (SiIP) were used as substrates, upon which Co₂P was coated using different concentrations of the precursor solutions, making the films with different thicknesses. The drop-cast cocatalyst forms a thinner layer on the top edges and a thicker layer at the vertices, which allows it to behave as p-Si at the top edge; hence effective light absorption is ensured while the thicker cocatalyst layer at the bottom ensures high catalytic efficiency. SiIP@Co₂P photocathodes exhibit a high photocurrent density of 35.2 mA cm⁻² at 0 V vs RHE and are stable over more than 150 h.⁹⁷ Corresponding results of thick and thin Co₂P cocatalysts over Si substrate are shown in Figure 6.

Table 2. Comparison of Performances Due to the Incorporation of Protective Coating or Cocatalyst Loading Reported in the Literature

photoelectrode	protective layer	electrolyte	V_{on} (V)	ΔV_{on} (V) = $V_{on}(\text{bare}) - V_{on}(\text{passivated})$	ref
Fe ₂ O ₃	IrO _x	0.1 M KH ₂ PO ₄ /K ₂ HPO ₄ (pH 7)	1.58	0.29	110
Fe ₂ O ₃	Co-P _i , 8–675 nm	0.2 M KCl, 0.1 M KH ₂ PO ₄ /K ₂ HPO ₄ (pH 6.9)	1.25	0.23	111
Fe ₂ O ₃	Ga ₂ O ₃ , tens of nm	1 M NaOH (pH 13.6)	1.02	0.25	112
Fe ₂ O ₃	Al ₂ O ₃ , tens of nm	1 M NaOH (pH 13.6)	1.02	0.07	112
Fe ₂ O ₃	In ₂ O ₃ , tens of nm	1 M NaOH (pH 13.6)	1.02	0.15	112
W:BiVO ₄	Co-P _i , 30 nm	0.1 M KH ₂ PO ₄ /K ₂ HPO ₄ (pH 8)	0.74	0.44	113
n-BiVO ₄ (nanoporous)	FeOOH/NiOOH	1 M KB _i with 0.1 M V ₂ O ₅ (pH 9.3)	0.2	–	114
TaON	IrO _x nanoparticles	1 M Na ₂ SO ₄ (pH 6)	0.15	0.40	115
n-WO ₃	Co-P _i	0.1 M KH ₂ PO ₄ (pH 7)	0.41	0.17	116
BiVO ₄	NiFe-LDH/MoO _x	0.1 M KH ₂ PO ₄ /K ₂ HPO ₄	–	267 mV	117
Ti@Fe ₂ O ₃	TiO ₂ /N ₂	1 M KOH	0.93	0.13	118
p-Si	Al ₂ O ₃ , 1.1–4.6 nm	0.5 M H ₂ SO ₄	–0.45	0.17	27
NiFeOx/B/BiVO ₄	borate	borate buffer (pH 9.5)	0.32	0.19	119

**Figure 8.** (A) Experimental setup for the SECM experiments and (B) feedback responses from the SECM approach plots used in generating the surface charge transfer kinetics. Reprinted from ref 120. Copyright 2021 Elsevier B.V.

For the enhancement in the catalytic performance of Cu₂O, one of the most promising photocathodes, the earth abundant aluminum nanoscale underlayer, is applied for the injection of hot electrons generated by surface plasmon photoexcitation into the conduction band of Cu₂O, followed by an overlayer of NiS to facilitate charge separation as it reduces the charge carrier built up in the Cu₂O layer by aiding charge carrier collection. The results are shown in Figure 7. While the pristine Cu₂O showed a photocurrent density of 0.57 mA cm⁻², the Al/Cu₂O/NiS electrode showed a 9 times greater photocurrent density of 5.16 mA cm⁻² at 0 V vs RHE.

The mechanism of action of NiS is described by eqs 15 and 16, where HNiS is formed by NiS and H⁺ via electron capture, which follows the same reaction to regenerate NiS by producing H₂.⁹⁸



Detailed investigations have been carried out on cocatalyst developments, dedicated toward the photoelectrochemical OER. As discussed earlier, BiVO₄, Fe₂O₃, and WO₃ are among the most researched photoanodes and several cocatalysts have been designed to facilitate the charge transfer process involving

these anodes. In this context, several transition metal oxides, layered oxyhydroxides, metal–organic framework derived oxides have been used as cocatalysts.^{53–63}

Surface modification of BiVO₄ was carried out using oxygen evolution catalysts (OEC) to accelerate the OER kinetics as well as to suppress the surface charge recombination. A number of the OEC such as Co-P_i,^{99–102} Co-B_i,^{103–105} NiOOH/Ni-borate,¹⁰⁶ FeOOH,¹⁰⁷ Ni(Fe)OOH,¹⁰⁸ and FeOOH/NiOOH¹⁰⁹ have been investigated. The catalysts indicated the improvement in the onset potential and the suppression of the charge recombination for the PEC water oxidation. The Co based cocatalyst, especially cobalt borate (Co-B_i), has been very popular among scientists and has been extensively investigated. Xue et al. have reported about the improved photocatalytic activity of the Co-B_i modified BiVO₄.¹⁰⁵ The ultrathin films of Co-B_i were able to be deposited due to the conformal TiO₂ films over undoped BiVO₄ material. Conformal TiO₂ has an additional role in stabilizing BiVO₄ and also Co-B_i. A few more examples of the enhancement in the catalytic performance due to the protective layer coating and also due to the cocatalyst loading are placed in Table 2.

The enhancement of the catalytic performance upon incorporation of Co-B_i and enhancement in the surface charge transfer kinetics have been reported by Kumar et al.^{31,120} The

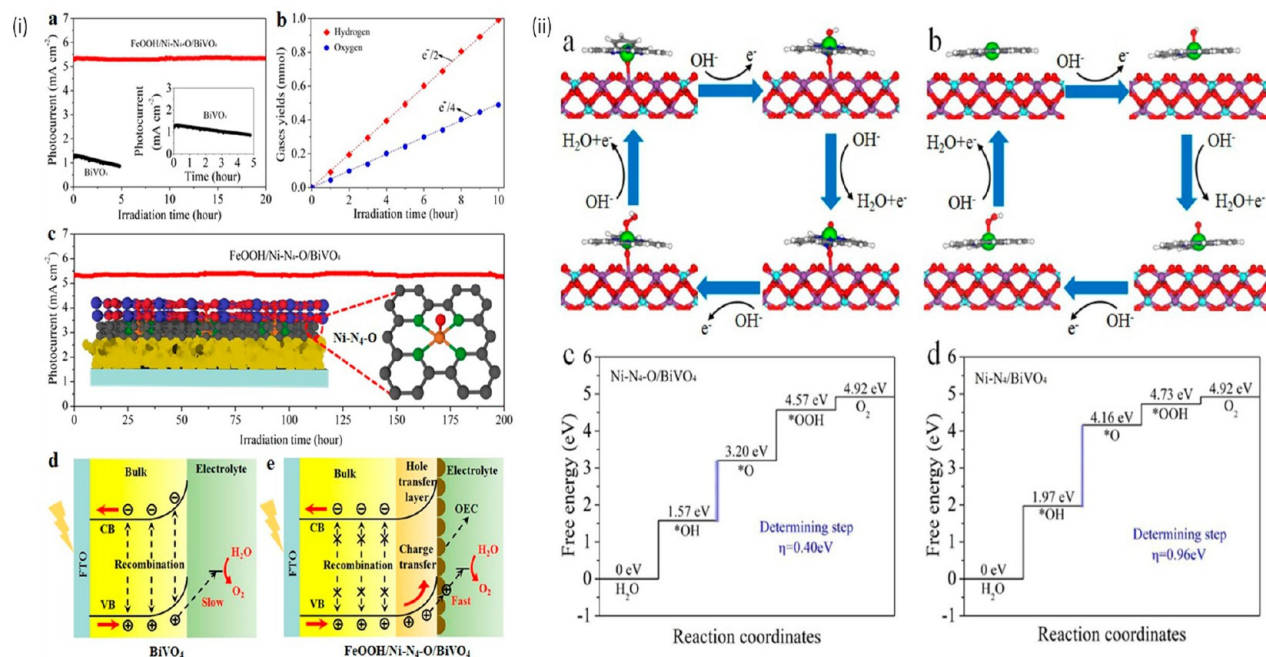


Figure 9. (i) PEC performance of BiVO_4 and $\text{FeOOH}/\text{Ni}-\text{N}_4-\text{O}/\text{BiVO}_4$ photoanodes at 1.0 V vs RHE under AM 1.5G simulated sunlight: (a) photocurrent density stabilities of BiVO_4 and $\text{FeOOH}/\text{Ni}-\text{N}_4-\text{O}/\text{BiVO}_4$ photoanodes; (b) plots of the theoretical charge number obtained from the $J-t$ curves and the actual quantities of H_2 and O_2 evolution of $\text{FeOOH}/\text{Ni}-\text{N}_4-\text{O}/\text{BiVO}_4$ photoanode; (c) long-term stability of $\text{FeOOH}/\text{Ni}-\text{N}_4-\text{O}/\text{BiVO}_4$ photoanode; (d, e) illustrations of the charge transfer process for BiVO_4 and $\text{FeOOH}/\text{Ni}-\text{N}_4-\text{O}/\text{BiVO}_4$ photoanodes. (ii) Origin of OER activity: (a, b) chemisorption models and (c, d) corresponding Gibbs free energies of $\text{Ni}-\text{N}_4-\text{O}/\text{BiVO}_4$ and $\text{Ni}-\text{N}_4/\text{BiVO}_4$. Reprinted from ref 124. Copyright 2021 American Chemical Society.

interfacial charge transfer kinetics has been investigated using scanning electrochemical microscopy (SECM) to quantify the effect of incorporation of Co- B_i on the BiVO_4 based photoanodes. The photogenerated holes on the BiVO_4 interface oxidize the ferrocyanide to ferricyanide redox probe which generates a feedback loop to the probe electrode of the SECM. The kinetic parameter, i.e., normalized apparent heterogeneous charge transfer rate constant k , has been obtained by fitting approach curves of SECM. The effective heterogeneous hole transfer rate constant k_{eff} for the oxidation of ferrocyanide to ferricyanide at the interface is calculated on the basis of normalized apparent heterogeneous charge transfer rate constant k with the equation $k_{\text{eff}} = \kappa D_{\text{diffusion}}/r_T$, where $D_{\text{diffusion}}$ is the diffusion coefficient of the redox probe and r_T is the radius of the ultramicroelectrode (UME). There is 33% improvement in k_{eff} at 0.4 V (vs Ag/AgCl) upon Co- B_i incorporation on the BiVO_4 , suggesting an enhancement in the interfacial charge transfer kinetics. The observation supports the assumption that Co- B_i facilitates the hole transfer by capturing holes and transferring them to the water molecule for oxidation. The schematics used in obtaining the surface charge transfer kinetics and the feedback responses used in generating the effective charge transfer rate constants using SECM are shown in Figure 8. The SECM feedback responses are shown for Co- B_i on BiVO_4 after the photocharging treatments.¹²⁰

Charge carriers are extracted from the semiconductor layer to the electrolyte via a cocatalyst layer, and the affinity of the charge carriers toward the cocatalyst and ease of subsequent transfer to the electrolyte are the key behind the enhanced charge injection. However, the effect of the formation of a suitable interface between the photoanode and the cocatalyst is often overlooked. With careful engineering at the atomistic level, coordination between the photoanode and the cocatalyst via a chemical bond

will enhance the effectiveness of charge transfer. Zhang et al.¹²⁴ reported a Ni based atomically dispersed $\text{Ni}-\text{N}_4$ cocatalyst linked to a BiVO_4 photoanode via an axial $\text{Ni}-\text{N}_4-\text{O}$ bond; some of the representative results are shown in Figure 9. It is observed that the charge separation in the photoanode is improved while the FeOOH cocatalyst layer is incorporated. The cocatalyst loaded $\text{Ni}-\text{N}_4-\text{O}/\text{BiVO}_4$ photoanode exhibited a photocurrent of 6 mA cm^{-2} at 1.23 V vs RHE, one of the highest reported photocurrents to date. The fabricated electrode was stable for more than 200 h of solar illumination at 1 V vs RHE without any obvious decay in photocurrent density, signifying robustness toward photocorrosion. The origin of enhanced OER activity has been investigated by theoretical studies using DFT. Findings of DFT suggest overpotential associated with the rate-determining step which involves the transformation of HO^* to O^* is decreased from 0.96 to 0.40 eV due to the formation of a Bi-O-Ni chemical bonding bridge. This bridge between the photoanode and the cocatalyst paves the way for the transfer of photogenerated charges.⁸

Apart from the atomistic distribution of cocatalyst, doping of cocatalysts like NiFeOOH with a lower electronegative atom like N enriches the metal centers like Ni and Fe with higher electron density, which is donated back to V centers and restrains the dissolution of V^{5+} centers. Hence, the stability of the photoanode can be dramatically enhanced. Zhang et al.⁸ synthesized a $\text{BiVO}_4/\text{N}:\text{NiFeO}_x$ photoanode, which showed an outstanding photocurrent density of 6.4 mA cm^{-2} at 1.23 V_{RHE} . Additionally, the effect of N incorporation on the relative concentrations of $\text{V}^{(5-x)+}$, Ni^{3+} , and Fe^{3+} is well depicted from an XPS study. Increase in the relative concentration of Fe^{3+} in $\text{BiVO}_4/\text{N}:\text{NiFeO}_x$ with respect to $\text{BiVO}_4/\text{NiFeO}_x$ with a decrease in Fe^{3+} and the appearance of $\text{V}^{(5-x)+}$ suggests increased electron availability at metal centers and the donation

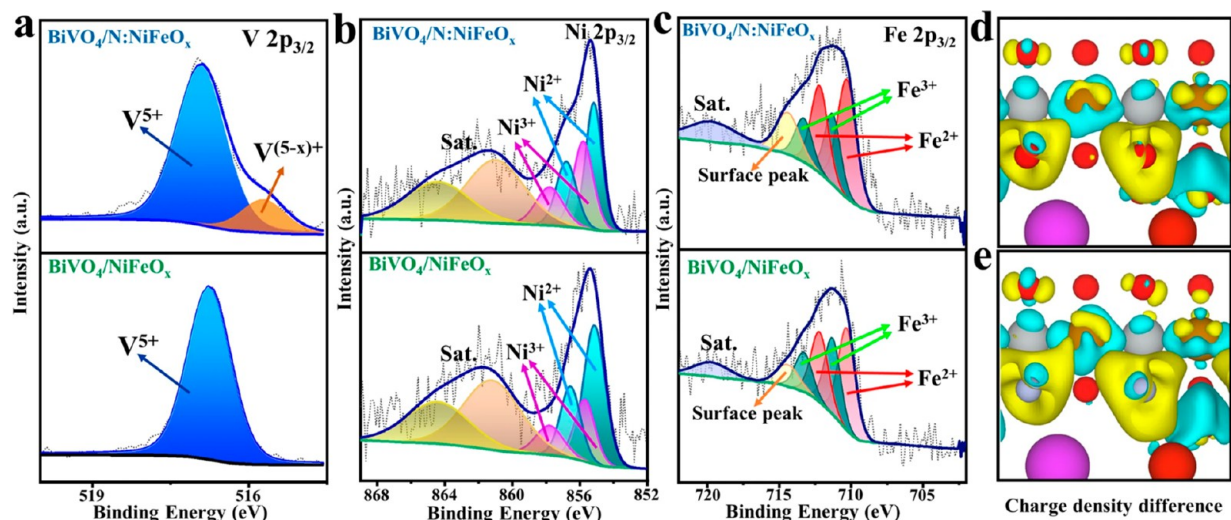


Figure 10. XPS high-resolution (a) V 2p, (b) Ni 2p, and (c) Fe 2p spectra for $\text{BiVO}_4/\text{N}:\text{NiFeO}_x$ and $\text{BiVO}_4/\text{NiFeO}_x$ photoanodes, respectively. Schematic of charge density difference (yellow and cyan represent charge accumulation and depletion, respectively; the cutoff of the density difference isosurface is 0.01 \AA^{-3}) of $\text{BiVO}_4/\text{NiFeO}_x$ (d) and $\text{BiVO}_4/\text{N}:\text{NiFeO}_x$ (e). From ref 8. CC BY 4.0.

of electrons from Ni centers to the V center. The process has a positive impact on the catalytic efficiency as represented in Figure 10.⁸

The modification of the surface states holds the key in generating the surface engineered materials with enhanced performance and stability of the catalysts. On the basis of the microkinetics model and simulations, the capacitances from the surface electronic states are evaluated, and the representative results from theoretical investigations are shown in Figure 11.¹²¹ The microkinetics model resulted in the capacitances of i-SS and r-SS, which are essentially measures of surface charge densities. The presence of surface charge densities corresponding to r-SS resulted in the retardation in photocurrent and the enhancement in the onset potential of the PEC process. The deviation in the Mott–Schottky plot has been observed below the onset potential, and this deviation resulted due to the r-SS assisted Fermi level pinning. The r-SS is responsible for the decrease in potential in the space charge region, and this lowering of potential resulted in the decrease in current density and increase in the onset potential. Therefore, it has been inferred that the r-SS reduces the performance of the photoanode and it is essential to remove such detrimental states. High temperature annealing is one of the ways to remove r-SS.¹²² The ALD- TiO_2 outer layer formation also has a positive role in modulating the r-SS and enhancing the PEC performance of the photoanodes.⁸⁷

At this juncture, an article¹¹ about the possibility of solar driven water splitting devices being a success or not is worth mentioning. The article mentioned the efficiency, robustness, and scalability of the device, and the device design and engineering aspects were given emphasis along with the material developments.¹¹ Afterward, several laboratories across the globe have reported results in this complicated and important branch of science in the sustainable generation of hydrogen using solar light. With several modifications of the materials through doping, heterojunction formation, morphology control, and surface modifications, the efficiency of the photoanodes has been improved significantly. However, the solar to hydrogen efficiency still requires improvement. Effective research has been carried out on the materials aspects of the PEC catalytic system by taking into consideration a better synthesis protocol, crystal facet engineering, suitable doping, heterojunction formation,

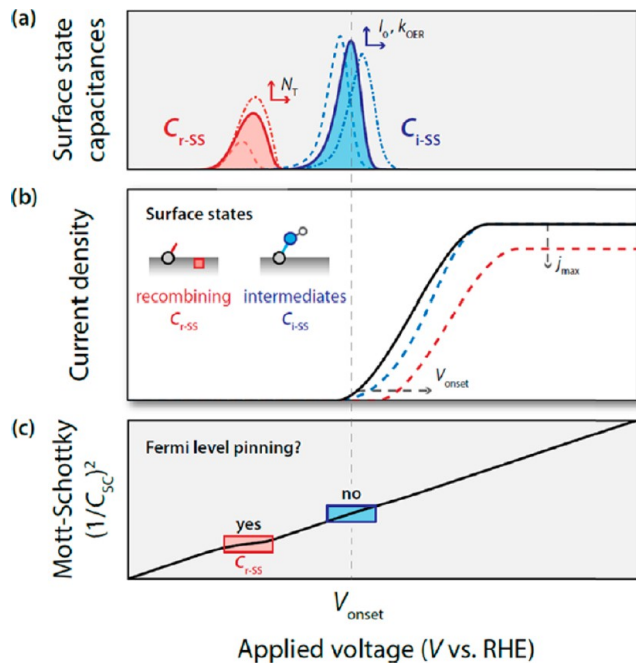


Figure 11. (a) Representative plot showing the relative magnitudes and positions of surface state capacitances (C_{r-SS} and C_{i-SS}) along the potential axis. For an increase in NT, the maximum of C_{r-SS} increases and shifts to higher potential as NT is increased. The maximum of C_{i-SS} depends on the illumination intensity (I_0) and the rate constants of the intermediate steps in the OER. (b) j - V characteristic showing an increase in onset potential and a decrease in saturation current density with an increase in C_{r-SS} ; the onset potential increases with a decrease in C_{i-SS} . (c) Mott–Schottky plot shows Fermi level pinning corresponding to r-SS and no Fermi level pinning corresponding to i-SS; the flattening in the Mott–Schottky plot observed around the onset potential is related to potential drop over. Reprinted from ref 121. Copyright 2020 American Chemical Society.

inclusion of the oxygen evolution catalysts at the surface, postsynthetic treatments, and enhancement of the surface reactivity. The stability of the catalytic system has been improved through the reduction of photocorrosion and chemical corrosion; ALD plays an important role in this part.

The challenge is to scale up the catalytic process for efficient, stable, and safe generation of hydrogen through the PEC route. The PEC route of generation of hydrogen is one of the green routes. The enhancement of efficiency and improving cost effectiveness are required for its commercialization. The U.S. Department of Energy has targeted the cost of hydrogen in the range \$2–4/kg of hydrogen; achieving this target requires the suitable assembly of catalytic systems for engineered upscaling.¹²³

An artificial intelligence and machine learning tool would play an important role in assembling and in geometry optimization for scale-up. Therefore, the combination of suitable policies along with multidimensional technological developments will make the generation of hydrogen through the photoelectrochemical route using a bismuth vanadate based catalytic system a success.

4. CONCLUSION

The performance of the semiconductor alone in the photoelectrode may not be sufficient in generating the efficient catalytic system suitable for practical applications. The semiconductor requires supports from several modifications, like heterojunction formation, bulk cocatalysts, surface cocatalysts, surface protective layer, and photocharging, to improve the performance. The present paper discussed the improvement in the photoelectrochemical catalysis processes by improving the surfaces of the catalysts.

The generation of engineered surfaces has been discussed with the generation of materials through crystal facet engineering, surface thin films, and surface cocatalyst loading. The crystal facet engineering procedure has the ability to generate the preferred surfaces with better catalytic performances from the same material. The surface thin film generation has the dual role in stabilization of the catalytic system from photocorrosion and the enhancement of the catalytic performance. The surface treatments from the ALD have been promising with its important role in the modulation of the surface electronic states of the catalysts. The importance of the surface states (i-SS and r-SS) has been discussed in the enhancement of the catalytic performances. The existence of the cocatalysts as surface layers has an important contribution in the efficient transfer of holes or electrons to the solution in the photoanode and photocathode, respectively. The modification of the surface electronic states holds the key to the enhancement of the catalytic performance by the efficient transfer of the minority carrier in either the photoanode or photocathode. The surface electronic states and the related kinetic parameters could be obtained from the electrochemical and spectroelectrochemical measurements with meaning related to the practical application. The theoretical calculations and modeling on the positioning of the surface electronic states support the electrochemical measurements, and the updated knowledge about the surface states holds the key to designing an efficient surface engineered catalytic system for prolonged water splitting applications.

AUTHOR INFORMATION

Corresponding Authors

Ashis Kumar Satpati – Analytical Chemistry Division, Bhabha Atomic Research Centre, Mumbai 400085, India; Homi Bhabha National Institute, Mumbai 400094, India;
orcid.org/0000-0002-2732-8706; Email: asatpati@barc.gov.in

Avesh Kumar Tyagi – Homi Bhabha National Institute, Mumbai 400094, India; Chemistry Group, Bhabha Atomic Research Centre, Mumbai 400085, India; orcid.org/0000-0002-4268-1364; Email: aktyagi@barc.gov.in

Authors

Sudipa Manna – Analytical Chemistry Division, Bhabha Atomic Research Centre, Mumbai 400085, India; Homi Bhabha National Institute, Mumbai 400094, India

Chandra Nath Patra – Analytical Chemistry Division, Bhabha Atomic Research Centre, Mumbai 400085, India; Homi Bhabha National Institute, Mumbai 400094, India

Complete contact information is available at:

<https://pubs.acs.org/10.1021/acsomega.3c07867>

Notes

The authors declare no competing financial interest.

ACKNOWLEDGMENTS

The authors thank Bhabha Atomic Research Centre (BARC) for fully funding the project.

REFERENCES

- (1) IEA. *Global Energy Review 2019*; IEA: Paris, 2020.
- (2) IEA. *Global Energy Review 2021*; IEA: Paris, 2021.
- (3) Ye, H.; Park, H. S.; Bard, A. J. Screening of Electrochemicals for Photoelectrochemical Water Oxidation on W-Doped BiVO₄ Photocatalysts by Scanning Electrochemical Microscopy. *J. Phys. Chem. C* **2011**, *115*, 12464–12470.
- (4) McCrory, C. C. L.; Jung, S.; Ferrer, I. M.; Chatman, S. M.; Peters, J. C.; Jaramillo, T. F. Benchmarking Hydrogen Evolving Reaction and Oxygen Evolving Reaction Electrocatalysts for Solar Water Splitting Devices. *J. Am. Chem. Soc.* **2015**, *137*, 4347–4357.
- (5) Cartagena, S.; Bedoya-Lora, F. E.; Calderón, J. A. Enhancement of anodically treated stainless steel by NiFeP-catalyst electrodeposition as bifunctional electrodes for water electrolysis. *J. Electrochem. Soc.* **2022**, *169*, No. 044501.
- (6) Lv, B.; Yang, Y.; Yang, C.; Huang, Z.; Zhou, Y.; Song, W.; Hao, J.; Shao, Z. Layered double hydroxide composite membrane for advanced alkaline water electrolysis. *International Journal of Energy Research* **2022**, *46*, 11892–11902.
- (7) Wang, T.; Wu, H.; Feng, C.; Zhang, L.; Zhang, J. MoP@ NiCo-LDH on nickel foam as bifunctional electrocatalyst for high efficiency water and urea–water electrolysis. *Journal of Materials Chemistry A* **2020**, *8*, 18106–18116.
- (8) Zhang, B.; Yu, S.; Dai, Y.; Huang, X.; Chou, L.; Lu, G.; Dong, G.; Bi, Y. Nitrogen-incorporation activates NiFeOx catalysts for efficiently boosting oxygen evolution activity and stability of BiVO₄ photoanodes. *Nat. Commun.* **2021**, *12*, 6969.
- (9) Jin, S.; Ma, X.; Pan, J.; Zhu, C.; Saji, S. E.; Hu, J.; Xu, X.; Sun, L.; Yin, Z. Oxygen vacancies activating surface reactivity to favor charge separation and transfer in nanoporous BiVO₄ photoanodes. *Applied Catalysis B: Environmental* **2021**, *281*, No. 119477.
- (10) Wang, Y.; Zhang, J.; Balogun, M. S.; Tong, Y.; Huang, Y. Oxygen vacancy-based metal oxides photoanodes in photoelectrochemical water splitting. *Materials Today Sustainability* **2022**, *18*, No. 100118.
- (11) McKone, J. R.; Lewis, N. S.; Gray, H. B. Will Solar-Driven Water-Splitting Devices See the Light of Day? *Chem. Mater.* **2014**, *26*, 407–414.
- (12) Lu, X.; Ye, K.-h.; Zhang, S.; Zhang, J.; Yang, J.; Huang, Y.; Ji, H. Amorphous type FeOOH modified defective BiVO₄ photoanodes for photoelectrochemical water oxidation. *Chemical Engineering Journal* **2022**, *428*, No. 131027.
- (13) Shi, X.; Wu, Q.; Cui, C. Modulating WO₃ Crystal Orientation to Suppress Hydroxyl Radicals for Sustainable Solar Water Oxidation. *ACS Catal.* **2023**, *13*, 1470–1476.

- (14) Wang, L.; Zhu, J.; Liu, X. Oxygen-Vacancy-Dominated Cocatalyst/Hematite Interface for Boosting Solar Water Splitting. *ACS Appl. Mater. Interfaces* **2019**, *11*, 22272–22277.
- (15) Zhang, X.; Klaver, P.; van Santen, R.; van de Sanden, M. C. M.; Bieberle-Hütter, A. Oxygen Evolution at Hematite Surfaces: The Impact of Structure and Oxygen Vacancies on Lowering the Overpotential. *J. Phys. Chem. C* **2016**, *120*, 18201–18208.
- (16) Cendula, P.; Bedoya-Lora, F. E.; Prabhakar, R. R. Semiconductor Catalysts for Oxygen and Hydrogen Evolution Reactions. *ACS Applied Energy Materials* **2022**, *5*, 14593–14604.
- (17) Thakur, A.; Ghosh, D.; Devi, P.; Kim, K.-H.; Kumar, P. Current progress and challenges in photoelectrode materials for the production of hydrogen. *Chemical Engineering Journal* **2020**, *397*, No. 125415.
- (18) Alley, O. J.; Wyatt, K.; Steiner, M. A.; Liu, G.; Kistler, T.; Zeng, G.; Larson, D. M.; Cooper, J. K.; Young, J. L.; Deutsch, T. G.; Toma, F. M. Best Practices in PEC Water Splitting: How to Reliably Measure Solar-to-Hydrogen Efficiency of Photoelectrodes. *Frontiers in Energy Research* **2022**, *10*, 884364.
- (19) Huang, M. H.; Naresh, G.; Chen, H.-S. Facet-Dependent Electrical, Photocatalytic, and Optical Properties of Semiconductor Crystals and Their Implications for Applications. *ACS Appl. Mater. Interfaces* **2018**, *10*, 4–15.
- (20) Clarizia, L.; Nadagouda, M. N.; Dionysiou, D. D. Recent advances and challenges of photoelectrochemical cells for hydrogen production. *Current Opinion in Green and Sustainable Chemistry* **2023**, *41*, No. 100825.
- (21) Kumaravel, V.; Imam, M. D.; Badreldin, A.; Chava, R. K.; Do, J. Y.; Kang, M.; Abdel-Wahab, A. Photocatalytic hydrogen production: role of sacrificial reagents on the activity of oxide, carbon, and sulfide catalysts. *Catalysts* **2019**, *9*, 276.
- (22) Kumar, M.; Meena, B.; Subramanyam, P.; Suryakala, D.; Subrahmanyam, C. Recent trends in photoelectrochemical water splitting: the role of cocatalysts. *NPG Asia Materials* **2022**, *14*, 88.
- (23) Dong, G.; Yan, L.; Bi, Y. Advanced oxygen evolution reaction catalysts for solar-driven photoelectrochemical water splitting. *Journal of Materials Chemistry A* **2023**, *11*, 3888–3903.
- (24) Hu, J.; Zhao, X.; Chen, W.; Su, H.; Chen, Z. Theoretical Insight into the Mechanism of Photoelectrochemical Oxygen Evolution Reaction on BiVO₄ Anode with Oxygen Vacancy. *J. Phys. Chem. C* **2017**, *121*, 18702–18709.
- (25) Wang, S.; Liu, G.; Wang, L. Crystal Facet Engineering of Photoelectrodes for Photoelectrochemical Water Splitting. *Chem. Rev.* **2019**, *119*, 5192–5247.
- (26) Browne, M. P.; Redondo, E.; Pumera, M. 3D Printing for Electrochemical Energy Applications. *Chem. Rev.* **2020**, *120*, 2783–2810.
- (27) Choi, M. J.; Jung, J.-Y.; Park, M.-J.; Song, J.-W.; Lee, J.-H.; Bang, J. H. Long-term durable silicon photocathode protected by a thin Al₂O₃/SiO_x layer for photoelectrochemical hydrogen evolution. *Journal of Materials Chemistry A* **2014**, *2*, 2928–2933.
- (28) Walter, M. G.; Warren, E. L.; McKone, J. R.; Boettcher, S. W.; Mi, Q.; Santori, E. A.; Lewis, N. S. Solar Water Splitting Cells. *Chem. Rev.* **2010**, *110*, 6446–6473.
- (29) Wang, Y.; Suzuki, H.; Xie, J.; Tomita, O.; Martin, D. J.; Higashi, M.; Kong, D.; Abe, R.; Tang, J. Mimicking Natural Photosynthesis: Solar to Renewable H₂ Fuel Synthesis by Z-Scheme Water Splitting Systems. *Chem. Rev.* **2018**, *118*, S201–S241.
- (30) Woods-Robinson, R.; Han, Y.; Zhang, H.; Ablekim, T.; Khan, I.; Persson, K. A.; Zakutayev, A. Correction to Wide Band Gap Chalcogenide Semiconductors. *Chem. Rev.* **2020**, *120*, 8035–8035.
- (31) Kumar, S.; Ahirwar, S.; Satpati, A. K. Insight into the PEC and interfacial charge transfer kinetics at the Mo doped BiVO₄ photoanodes. *RSC Adv.* **2019**, *9*, 41368–41382.
- (32) Yang, X.; Jiang, P.; Yu, Q.; Jiang, H.; Xu, X. Orderly decoupled dynamics modulation in nanoporous BiVO₄ photoanodes for solar water splitting. *J. Alloys Compd.* **2023**, *931*, No. 167428.
- (33) Xie, Y. P.; Liu, G.; Yin, L.; Cheng, H.-M. Crystal facet-dependent photocatalytic oxidation and reduction reactivity of monoclinic WO₃ for solar energy conversion. *J. Mater. Chem.* **2012**, *22*, 6746–6751.
- (34) Wang, X.; Yin, L.; Liu, G.; Wang, L.; Saito, R.; Lu, G. Q.; Cheng, H.-M. Polar interface-induced improvement in high photocatalytic hydrogen evolution over ZnO–CdS heterostructures. *Energy Environ. Sci.* **2011**, *4*, 3976–3979.
- (35) Chen, Y.; Zhang, L.; Ning, L.; Zhang, C.; Zhao, H.; Liu, B.; Yang, H. Superior photocatalytic activity of porous wurtzite ZnO nanosheets with exposed {001} facets and a charge separation model between polar (001) and (00 $\bar{1}$) surfaces. *Chemical Engineering Journal* **2015**, *264*, 557–564.
- (36) Wang, L.; Li, H.; Xu, S.; Yue, Q.; Liu, J. Facet-dependent optical properties of nanostructured ZnO. *Mater. Chem. Phys.* **2014**, *147*, 1134–1139.
- (37) Zhou, G.; Wu, X.; Liu, L.; Zhu, X.; Hao, Y.; Chu, P. K. Facet-controlled synthesis and facet-dependent photocatalytic properties of SnO₂ micropolyhedrons. *Appl. Surf. Sci.* **2015**, *349*, 798–804.
- (38) Kumar, S.; Parthasarathy, R.; Singh, A. P.; Wickman, B.; Thirumal, M.; Ganguli, A. K. Dominant {100} facet selectivity for enhanced photocatalytic activity of NaNbO₃ in NaNbO₃/CdS core/shell heterostructures. *Catalysis Science & Technology* **2017**, *7*, 481–495.
- (39) Liu, J.; Lu, W.; Tian, B.; Hu, B.; Jin, L.; Shi, Y.; Li, L.; Wang, Z. Shape-controlled synthesis and facet-dependent performance of single-crystal Bi₂₅GaO₃₉ photocatalysts. *CrystEngComm* **2016**, *18*, 7715–7721.
- (40) Hu, Y.; Chen, G.; Li, C.; Zhou, Y.; Sun, J.; Hao, S.; Han, Z. Fabrication of {010} facet dominant BiTaO₄ single-crystal nanoplates for efficient photocatalytic performance. *Journal of Materials Chemistry A* **2016**, *4*, 5274–5281.
- (41) Jiang, J.; Zhao, K.; Xiao, X.; Zhang, L. Synthesis and facet-dependent photoreactivity of BiOCl single-crystalline nanosheets. *J. Am. Chem. Soc.* **2012**, *134*, 4473–4476.
- (42) Li, H.; Xu, S.; Huang, Z.; Huang, J.; Wang, J.; Zhang, L.; Zhang, C. Facet-dependent nonlinear optical properties of bismuth oxychloride single-crystal nanosheets. *Journal of Materials Chemistry C* **2018**, *6*, 8709–8716.
- (43) Liu, G.; Wang, T.; Zhou, W.; Meng, X.; Zhang, H.; Liu, H.; Kako, T.; Ye, J. Crystal-facet-dependent hot-electron transfer in plasmonic-Au/semiconductor heterostructures for efficient solar photocatalysis. *Journal of materials chemistry C* **2015**, *3*, 7538–7542.
- (44) Selcuk, S.; Selloni, A. Facet-dependent trapping and dynamics of excess electrons at anatase TiO₂ surfaces and aqueous interfaces. *Nat. Mater.* **2016**, *15*, 1107–1112.
- (45) Zhu, J.; Fan, F.; Chen, R.; An, H.; Feng, Z.; Li, C. Direct imaging of highly anisotropic photogenerated charge separations on different facets of a single BiVO₄ photocatalyst. *Angew. Chem.* **2015**, *127*, 9239–9242.
- (46) Sun, X.; Zhang, Y.; Song, P.; Pan, J.; Zhuang, L.; Xu, W.; Xing, W. Fluorine-Doped Carbon Blacks: Highly Efficient Metal-Free Electrocatalysts for Oxygen Reduction Reaction. *ACS Catal.* **2013**, *3*, 1726–1729.
- (47) Chen, P.; Zhou, T.; Wang, S.; Zhang, N.; Tong, Y.; Ju, H.; Chu, W.; Wu, C.; Xie, Y. Dynamic migration of surface fluorine anions on cobalt-based materials to achieve enhanced oxygen evolution catalysis. *Angew. Chem., Int. Ed.* **2018**, *57*, 15471–15475.
- (48) Pan, F.; Li, B.; Xiang, X.; Wang, G.; Li, Y. Efficient CO₂ Electroreduction by Highly Dense and Active Pyridinic Nitrogen on Holey Carbon Layers with Fluorine Engineering. *ACS Catal.* **2019**, *9*, 2124–2133.
- (49) Zhang, B.; Chou, L.; Bi, Y. Tuning surface electronegativity of BiVO₄ photoanodes toward high-performance water splitting. *Applied Catalysis B: Environmental* **2020**, *262*, No. 118267.
- (50) Kuo, C.-H.; Yang, Y.-C.; Gwo, S.; Huang, M. H. Facet-dependent and Au nanocrystal-enhanced electrical and photocatalytic properties of Au–Cu₂O core–shell heterostructures. *J. Am. Chem. Soc.* **2011**, *133*, 1052–1057.
- (51) Kment, S.; Schmuki, P.; Hubicka, Z.; Machala, L.; Kirchgeorg, R.; Liu, N.; Wang, L.; Lee, K.; Olejnicek, J.; Cada, M.; Gregora, I.; Zboril, R. Photoanodes with Fully Controllable Texture: The Enhanced Water

Splitting Efficiency of Thin Hematite Films Exhibiting Solely (110) Crystal Orientation. *ACS Nano* **2015**, *9*, 7113–7123.

(52) Xie, Z.; Chen, D.; Zhai, J.; Huang, Y.; Ji, H. Charge separation via synergy of homojunction and electrocatalyst in BiVO₄ for photoelectrochemical water splitting. *Applied Catalysis B: Environmental* **2023**, *334*, No. 122865.

(53) Garg, P.; Mohapatra, L.; Poonia, A. K.; Kushwaha, A. K.; Adarsh, K. N. V. D.; Deshpande, U. Single Crystalline α -Fe₂O₃ Nanosheets with Improved PEC Performance for Water Splitting. *ACS Omega* **2023**, *8*, 38607–38618.

(54) Kment, S.; Riboni, F.; Pausova, S.; Wang, L.; Wang, L.; Han, H.; Hubicka, Z.; Krysa, J.; Schmuki, P.; Zboril, R. Photoanodes based on TiO₂ and α -Fe₂O₃ for solar water splitting—superior role of 1D nanoarchitectures and of combined heterostructures. *Chem. Soc. Rev.* **2017**, *46*, 3716–3769.

(55) Zhou, Y.; Zhang, L.; Lin, L.; Wygant, B. R.; Liu, Y.; Zhu, Y.; Zheng, Y.; Mullins, C. B.; Zhao, Y.; Zhang, X.; Yu, G. Highly efficient photoelectrochemical water splitting from hierarchical WO₃/BiVO₄ nanoporous sphere arrays. *Nano Lett.* **2017**, *17*, 8012–8017.

(56) Yao, B.; Zhang, J.; Fan, X.; He, J.; Li, Y. Surface engineering of nanomaterials for photoelectrochemical water splitting. *Small* **2019**, *15*, No. 1803746.

(57) Li, C.; Li, A.; Luo, Z.; Zhang, J.; Chang, X.; Huang, Z.; Wang, T.; Gong, J. Surviving high-temperature calcination: ZrO₂-induced hematite nanotubes for photoelectrochemical water oxidation. *Angew. Chem.* **2017**, *129*, 4214–4219.

(58) Dlugosch, T.; Chnani, A.; Muralidhar, P.; Schirmer, A.; Biskupek, J.; Strehle, S. Thermal oxidation synthesis of crystalline iron-oxide nanowires on low-cost steel substrates for solar water splitting. *Semicond. Sci. Technol.* **2017**, *32*, No. 084001.

(59) Wang, X.; Ma, S.; Liu, B.; Wang, S.; Huang, W. Imperfect makes perfect: defect engineering of photoelectrodes towards efficient photoelectrochemical water splitting. *Chem. Commun.* **2023**, *59*, 10044–10066.

(60) Su, J.; Feng, X.; Sloppy, J. D.; Guo, L.; Grimes, C. A. Vertically aligned WO₃ nanowire arrays grown directly on transparent conducting oxide coated glass: synthesis and photoelectrochemical properties. *Nano Lett.* **2011**, *11*, 203–208.

(61) Zhou, M.; Bao, J.; Xu, Y.; Zhang, J.; Xie, J.; Guan, M.; Wang, C.; Wen, L.; Lei, Y.; Xie, Y. Photoelectrodes based upon Mo: BiVO₄ inverse opals for photoelectrochemical water splitting. *ACS Nano* **2014**, *8*, 7088–7098.

(62) Dey, K. K.; Gahlawat, S.; Ingole, P. P. BiVO₄ optimized to nanoworm morphology for enhanced activity towards photoelectrochemical water splitting. *Journal of Materials Chemistry A* **2019**, *7*, 21207–21221.

(63) Zhang, H.; Cheng, C. Three-dimensional FTO/TiO₂/BiVO₄ composite inverse opals photoanode with excellent photoelectrochemical performance. *ACS Energy Letters* **2017**, *2*, 813–821.

(64) Xu, S.; Fu, D.; Song, K.; Wang, L.; Yang, Z.; Yang, W.; Hou, H. One-dimensional WO₃/BiVO₄ heterojunction photoanodes for efficient photoelectrochemical water splitting. *Chemical Engineering Journal* **2018**, *349*, 368–375.

(65) Zhou, Y.; Zhang, L.; Lin, L.; Wygant, B. R.; Liu, Y.; Zhu, Y.; Zheng, Y.; Mullins, C. B.; Zhao, Y.; Zhang, X.; Yu, G. Highly Efficient Photoelectrochemical Water Splitting from Hierarchical WO₃/BiVO₄ Nanoporous Sphere Arrays. *Nano Lett.* **2017**, *17*, 8012–8017.

(66) Ibadurrohman, M.; Hellgardt, K. Morphological Modification of TiO₂ Thin Films as Highly Efficient Photoanodes for Photoelectrochemical Water Splitting. *ACS Appl. Mater. Interfaces* **2015**, *7*, 9088–9097.

(67) Xia, M.; Zhao, X.; Lin, C.; Pan, W.; Zhang, Y.; Guo, Z.; Leung, D. Y. C. High-Voltage Etching-Induced Terrace-like WO₃ Photoanode for Efficient Photoelectrochemical Water Splitting. *ACS Applied Energy Materials* **2023**, *6*, 8717–8728.

(68) Dai, Y.; Xie, G.; Jia, X.; Guo, B.; Gong, J. R. Surface charge recombination matters for single-versus polycrystalline catalysts in the case study of hematite photoanodes. *Appl. Surf. Sci.* **2023**, *610*, No. 155501.

(69) Ahn, H.-J.; Kment, S.; Naldoni, A.; Zbořil, R.; Schmuki, P. Band gap and Morphology Engineering of Hematite Nanoflakes from an Ex Situ Sn Doping for Enhanced Photoelectrochemical Water Splitting. *ACS Omega* **2022**, *7*, 35109–35117.

(70) Xiao, J.; Li, C.; Jia, X.; Du, B.; Li, R.; Wang, B. Enabling high low-bias performance of Fe₂O₃ photoanode for photoelectrochemical water splitting. *J. Colloid Interface Sci.* **2023**, *633*, 555–565.

(71) Xu, X.; Jin, S.; Yang, C.; Pan, J.; Du, W.; Hu, J.; Zeng, H.; Zhou, Y. Engineering Interfaces to Steer Hole Dynamics of BiVO₄ Photoanodes for Solar Water Oxidation. *Solar RRL* **2019**, *3*, No. 1900115.

(72) Shyamal, S.; Hajra, P.; Mandal, H.; Bera, A.; Sariket, D.; Satpati, A. K.; Kundu, S.; Bhattacharya, C. Benign role of Bi on an electrodeposited Cu₂O semiconductor towards photo-assisted H₂ generation from water. *Journal of Materials Chemistry A* **2016**, *4*, 9244–9252.

(73) Chen, S.; Wang, L.-W. Thermodynamic Oxidation and Reduction Potentials of Photocatalytic Semiconductors in Aqueous Solution. *Chem. Mater.* **2012**, *24*, 3659–3666.

(74) Bak, T.; Nowotny, J.; Rekas, M.; Sorrell, C. C. Photoelectrochemical hydrogen generation from water using solar energy. Materials-related aspects. *International journal of hydrogen energy* **2002**, *27*, 991–1022.

(75) Gerischer, H. Electrolytic decomposition and photodecomposition of compound semiconductors in contact with electrolytes. *J. Vac. Sci. Technol.* **1978**, *15*, 1422–1428.

(76) Kafizas, A.; King, X.; Selim, S.; Mesa, C. A.; Ma, Y.; Burgess, C.; McLachlan, M. A.; Durrant, J. R. Ultra-thin Al₂O₃ coatings on BiVO₄ photoanodes: Impact on performance and charge carrier dynamics. *Catal. Today* **2019**, *321*, 59–66.

(77) Lichterman, M. F.; Shaner, M. R.; Handler, S. G.; Brunenschwig, B. S.; Gray, H. B.; Lewis, N. S.; Spurgeon, J. M. Enhanced stability and activity for water oxidation in alkaline media with bismuth vanadate photoelectrodes modified with a cobalt oxide catalytic layer produced by atomic layer deposition. *J. Phys. Chem. Lett.* **2013**, *4*, 4188–4191.

(78) Kim, T. W.; Choi, K.-S. Improving stability and photoelectrochemical performance of BiVO₄ photoanodes in basic media by adding a ZnFe₂O₄ layer. *J. Phys. Chem. Lett.* **2016**, *7*, 447–451.

(79) Zhang, Y.; Zhang, X.; Wang, D.; Wan, F.; Liu, Y. Protecting hydrogenation-generated oxygen vacancies in BiVO₄ photoanode for enhanced water oxidation with conformal ultrathin amorphous TiO₂ layer. *Appl. Surf. Sci.* **2017**, *403*, 389–395.

(80) McDowell, M. T.; Lichterman, M. F.; Spurgeon, J. M.; Hu, S.; Sharp, I. D.; Brunenschwig, B. S.; Lewis, N. S. Improved stability of polycrystalline bismuth vanadate photoanodes by use of dual-layer thin TiO₂/Ni coatings. *J. Phys. Chem. C* **2014**, *118*, 19618–19624.

(81) Zhong, M.; Hisatomi, T.; Kuang, Y.; Zhao, J.; Liu, M.; Iwase, A.; Jia, Q.; Nishiyama, H.; Minegishi, T.; Nakabayashi, M.; et al. Surface modification of CoO_x loaded BiVO₄ photoanodes with ultrathin p-type NiO layers for improved solar water oxidation. *J. Am. Chem. Soc.* **2015**, *137*, 5053–5060.

(82) Häggglund, C.; Apell, S. P.; Kasemo, B. Maximized Optical Absorption in Ultrathin Films and Its Application to Plasmon-Based Two-Dimensional Photovoltaics. *Nano Lett.* **2010**, *10*, 3135–3141.

(83) Han, J. W.; Jin, H. S.; Kim, Y. J.; Heo, J. S.; Kim, W.-H.; Ahn, J.-H.; Kim, J. H.; Park, T. J. Advanced Atomic Layer Deposition: Ultrathin and Continuous Metal Thin Film Growth and Work Function Control Using the Discrete Feeding Method. *Nano Lett.* **2022**, *22*, 4589–4595.

(84) Satpati, A. K.; Arroyo-Currás, N.; Ji, L.; Yu, E. T.; Bard, A. J. Electrochemical Monitoring of TiO₂ Atomic Layer Deposition by Chronoamperometry and Scanning Electrochemical Microscopy. *Chem. Mater.* **2013**, *25*, 4165–4172.

(85) Le Formal, F.; Tétreault, N.; Cornuz, M.; Moehl, T.; Grätzel, M.; Sivula, K. Passivating surface states on water splitting hematite photoanodes with alumina overlayers. *Chemical Science* **2011**, *2*, 737–743.

(86) Li, X.; Bassi, P. S.; Boix, P. P.; Fang, Y.; Wong, L. H. Revealing the role of TiO₂ surface treatment of hematite nanorods photoanodes for solar water splitting. *ACS Appl. Mater. Interfaces* **2015**, *7*, 16960–16966.

- (87) Sharma, A.; Manna, S.; Satpati, A. K. Enhancement in Photoelectrochemical Efficiency and Modulation of Surface States in BiVO₄ through the TiO₂ Outer Layer Using the Atomic Layer Deposition Technique. *J. Phys. Chem. C* **2023**, *127*, 4395–4406.
- (88) Yang, J.; Wang, D.; Han, H.; Li, C. A. N. Roles of cocatalysts in photocatalysis and photoelectrocatalysis. *Accounts of chemical research* **2013**, *46*, 1900–1909.
- (89) Nandjou, F.; Haussener, S. Kinetic Competition between Water-Splitting and Photocorrosion Reactions in Photoelectrochemical Devices. *ChemSusChem* **2019**, *12*, 1984–1994.
- (90) Ding, C.; Shi, J.; Wang, Z.; Li, C. Photoelectrocatalytic water splitting: significance of cocatalysts, electrolyte, and interfaces. *ACS catalysis* **2017**, *7*, 675–688.
- (91) Ma, P.; Wang, D. The principle of photoelectrochemical water splitting. *Nanomaterials for Energy Conversion and Storage*; Wang, D., Cao, G., Eds.; World Scientific: 2018; pp 1–61. DOI: 10.1142/9781786343635_0001.
- (92) Zhang, S.; Zhao, H.; Li, X.; Li, Y.; Jin, Y.; Liu, X.; Shi, G.; Wong, P. K. A hierarchical SiPN/CN/MoS_x photocathode with low internal resistance and strong light-absorption for solar hydrogen production. *Applied Catalysis B: Environmental* **2022**, *300*, No. 120758.
- (93) Vijselaar, W.; Westerik, P.; Veerbeek, J.; Tiggelaar, R. M.; Berenschot, E.; Tas, N. R.; Gardeniers, H.; Huskens, J. Spatial decoupling of light absorption and catalytic activity of Ni–Mo-loaded high-aspect-ratio silicon microwire photocathodes. *Nature Energy* **2018**, *3*, 185–192.
- (94) Kang, D.; Young, J. L.; Lim, H.; Klein, W. E.; Chen, H.; Xi, Y.; Gai, B.; Deutsch, T. G.; Yoon, J. Printed assemblies of GaAs photoelectrodes with decoupled optical and reactive interfaces for unassisted solar water splitting. *Nature Energy* **2017**, *2*, 17043.
- (95) Vijselaar, W.; Tiggelaar, R. M.; Gardeniers, H.; Huskens, J. Efficient and Stable Silicon Microwire Photocathodes with a Nickel Silicide Interlayer for Operation in Strongly Alkaline Solutions. *ACS Energy Letters* **2018**, *3*, 1086–1092.
- (96) Bae, D.; Pedersen, T.; Seger, B.; Malizia, M.; Kuznetsov, A.; Hansen, O.; Chorkendorff, I.; Vesborg, P. C. K. Back-illuminated Si photocathode: a combined experimental and theoretical study for photocatalytic hydrogen evolution. *Energy Environ. Sci.* **2015**, *8*, 650–660.
- (97) Thalluri, S. M.; Wei, B.; Welter, K.; Thomas, R.; Smirnov, V.; Qiao, L.; Wang, Z.; Finger, F.; Liu, L. Inverted Pyramid Textured p-Silicon Covered with Co₂P as an Efficient and Stable Solar Hydrogen Evolution Photocathode. *ACS Energy Letters* **2019**, *4*, 1755–1762.
- (98) Chen, D.; Liu, Z.; Guo, Z.; Yan, W.; Ruan, M. Decorating Cu₂O photocathode with noble-metal-free Al and NiS cocatalysts for efficient photoelectrochemical water splitting by light harvesting management and charge separation design. *Chemical Engineering Journal* **2020**, *381*, No. 122655.
- (99) Abdi, F. F.; Firet, N.; van de Krol, R. Efficient BiVO₄ thin film photoanodes modified with Cobalt Phosphate catalyst and W-doping. *ChemCatChem* **2013**, *5*, 490–496.
- (100) Nellist, M. R.; Qiu, J.; Laskowski, F. A.; Toma, F. M.; Boettcher, S. W. Potential-sensing electrochemical AFM shows CoPi as a hole collector and oxygen evolution catalyst on BiVO₄ water-splitting photoanodes. *ACS Energy Letters* **2018**, *3*, 2286–2291.
- (101) Pilli, S. K.; Furtak, T. E.; Brown, L. D.; Deutsch, T. G.; Turner, J. A.; Herring, A. M. Cobalt-phosphate (Co-Pi) catalyst modified Mo-doped BiVO₄ photoelectrodes for solar water oxidation. *Energy Environ. Sci.* **2011**, *4*, 5028–5034.
- (102) Zhong, D. K.; Choi, S.; Gamelin, D. R. Near-complete suppression of surface recombination in solar photoelectrolysis by “Co-Pi” catalyst-modified W: BiVO₄. *J. Am. Chem. Soc.* **2011**, *133*, 18370–18377.
- (103) Ding, C.; Shi, J.; Wang, D.; Wang, Z.; Wang, N.; Liu, G.; Xiong, F.; Li, C. Visible light driven overall water splitting using cocatalyst/BiVO₄ photoanode with minimized bias. *Phys. Chem. Chem. Phys.* **2013**, *15*, 4589–4595.
- (104) Wang, S.; Chen, P.; Yun, J. H.; Hu, Y.; Wang, L. An electrochemically treated BiVO₄ photoanode for efficient photoelectrochemical water splitting. *Angew. Chem., Int. Ed.* **2017**, *56*, 8500–8504.
- (105) Xue, D.; Kan, M.; Qian, X.; Zhao, Y. A Tandem Water Splitting Cell Based on Nanoporous BiVO₄ Photoanode Cocatalyzed by Ultrasmall Cobalt Borate Sandwiched with Conformal TiO₂ Layers. *ACS Sustainable Chem. Eng.* **2018**, *6*, 16228–16234.
- (106) Choi, S. K.; Choi, W.; Park, H. Solar water oxidation using nickel-borate coupled BiVO₄ photoelectrodes. *Phys. Chem. Chem. Phys.* **2013**, *15*, 6499–6507.
- (107) Ge, G.; Liu, M.; Liu, C.; Zhou, W.; Wang, D.; Liu, L.; Ye, J. Ultrathin FeOOH nanosheets as an efficient cocatalyst for photocatalytic water oxidation. *Journal of materials chemistry A* **2019**, *7*, 9222–9229.
- (108) Zhang, X.; Li, H.; Kong, W.; Liu, H.; Fan, H.; Wang, M. Reducing the surface recombination during light-driven water oxidation by core-shell BiVO₄@ Ni: FeOOH. *Electrochim. Acta* **2019**, *300*, 77–84.
- (109) Kim, T. W.; Choi, K.-S. Nanoporous BiVO₄ photoanodes with dual-layer oxygen evolution catalysts for solar water splitting. *Science* **2014**, *343*, 990–994.
- (110) Badia-Bou, L.; Mas-Marza, E.; Rodenas, P.; Barea, E. M.; Fabregat-Santiago, F.; Gimenez, S.; Peris, E.; Bisquert, J. Water Oxidation at Hematite Photoelectrodes with an Iridium-Based Catalyst. *J. Phys. Chem. C* **2013**, *117*, 3826–3833.
- (111) Klahr, B.; Gimenez, S.; Fabregat-Santiago, F.; Bisquert, J.; Hamann, T. W. Photoelectrochemical and Impedance Spectroscopic Investigation of Water Oxidation with “Co–Pi”-Coated Hematite Electrodes. *J. Am. Chem. Soc.* **2012**, *134*, 16693–16700.
- (112) Hisatomi, T.; Le Formal, F.; Cornuz, M.; Brillet, J.; Tétreault, N.; Sivula, K.; Grätzel, M. Cathodic shift in onset potential of solar oxygen evolution on hematite by 13-group oxide overlayers. *Energy Environ. Sci.* **2011**, *4*, 2512–2515.
- (113) Zhong, D. K.; Choi, S.; Gamelin, D. R. Near-Complete Suppression of Surface Recombination in Solar Photoelectrolysis by “Co-Pi” Catalyst-Modified W:BiVO₄. *J. Am. Chem. Soc.* **2011**, *133*, 18370–18377.
- (114) Lee, D. K.; Choi, K.-S. Enhancing long-term photostability of BiVO₄ photoanodes for solar water splitting by tuning electrolyte composition. *Nature Energy* **2018**, *3*, 53–60.
- (115) Abe, R.; Higashi, M.; Domen, K. Facile Fabrication of an Efficient Oxynitride TaON Photoanode for Overall Water Splitting into H₂ and O₂ under Visible Light Irradiation. *J. Am. Chem. Soc.* **2010**, *132*, 11828–11829.
- (116) Seabold, J. A.; Choi, K.-S. Effect of a Cobalt-Based Oxygen Evolution Catalyst on the Stability and the Selectivity of Photo-Oxidation Reactions of a WO₃ Photoanode. *Chem. Mater.* **2011**, *23*, 1105–1112.
- (117) Kang, B.; Bilal Hussain, M.; Cheng, X.; Peng, C.; Wang, Z. Green electrodeposition synthesis of NiFe-LDH/MoO_x/BiVO₄ for efficient photoelectrochemical water splitting. *J. Colloid Interface Sci.* **2022**, *626*, 146–155.
- (118) Devi, H. R.; Ong, B. C.; Zhao, X.; Dong, Z.; Nanda, K. K.; Chen, Z. Insights into Improving Photoelectrochemical Water-Splitting Performance Using Hematite Anode. *Energy Technology* **2022**, *10*, No. 2100457.
- (119) Zhang, J.; Huang, Y.; Lu, X.; Yang, J.; Tong, Y. Enhanced BiVO₄ Photoanode Photoelectrochemical Performance via Borate Treatment and a NiFeO_x Cocatalyst. *ACS Sustainable Chem. Eng.* **2021**, *9*, 8306–8314.
- (120) Kumar, S.; Satpati, A. K. Investigation of interfacial charge transfer kinetics of photocharged Co-Bi modified BiVO₄ using scanning electrochemical microscopy (SECM). *Electrochim. Acta* **2021**, *368*, No. 137565.
- (121) George, K.; Khachatryan, T.; van Berkel, M.; Sinha, V.; Bieberle-Hütter, A. Understanding the Impact of Different Types of Surface States on Photoelectrochemical Water Oxidation: A Microkinetic Modeling Approach. *ACS Catal.* **2020**, *10*, 14649–14660.

(122) Zandi, O.; Hamann, T. W. Enhanced Water Splitting Efficiency Through Selective Surface State Removal. *J. Phys. Chem. Lett.* **2014**, *5*, 1522–1526.

(123) DOE Technical Targets for Hydrogen Production from Photoelectrochemical Water Splitting. Office of Energy Efficiency & Renewable Energy, U.S. Department of Energy. <https://www.energy.gov/eere/fuelcells/doe-technical-targets-hydrogen-production-photoelectrochemical-water-splitting>.

(124) Zhang, X.; Zhai, P.; Zhang, Y.; Wu, Y.; Wang, C.; Ran, L.; Gao, J.; Li, Z.; Zhang, B.; Fan, Z.; Sun, L.; Hou, J. Engineering Single-Atomic Ni-N₄-O Sites on Semiconductor Photoanodes for High-Performance Photoelectrochemical Water Splitting. *J. Am. Chem. Soc.* **2021**, *143*, 20657–20669.